Aus dem Zentrum für Kinder- und Jugendmedizin
der Universität zu Köln
Klinik und Poliklinik für Kinder- und Jugendmedizin
Direktor: Universitätsprofessor Dr. med. J. Dötsch

Tracing tumor evolution in ganglioneuroblastoma, nodular subtype

Inaugural-Dissertation zur Erlangung der Doktorwürde
der Medizinischen Fakultät
der Universität zu Köln

vorgelegt von
Tancia Garcia

promoviert am 26.02.2024

Gedruckt mit Genehmigung der Medizinischen Fakultät der Universität zu Köln

Druckjahr 2024

Dekan: Universitätsprofessor Dr. med. G. R. Fink
1. Gutachter: Universitätsprofessor Dr. med. M. Fischer
2. Gutachter: Professor Dr. rer. nat. M. Montesinos-Rongen

Erklärung

Ich erkläre hiermit, dass ich die vorliegende Dissertationsschrift ohne unzulässige Hilfe Dritter und ohne Benutzung anderer als der angegebenen Hilfsmittel angefertigt habe; die aus fremden Quellen direkt oder indirekt übernommenen Gedanken sind als solche kenntlich gemacht.

Bei der Auswahl und Auswertung des Materials sowie bei der Herstellung des Manuskriptes habe ich Unterstützungsleistungen von folgenden Personen erhalten:

Herr Dr. Justus Ackermann

Weitere Personen waren an der Erstellung der vorliegenden Arbeit nicht beteiligt. Insbesondere habe ich nicht die Hilfe einer Promotionsberaterin/eines Promotionsberaters in Anspruch genommen. Dritte haben von mir weder unmittelbar noch mittelbar geldwerte Leistungen für Arbeiten erhalten, die im Zusammenhang mit dem Inhalt der vorgelegten Dissertationsschrift stehen.

Die Dissertationsschrift wurde von mir bisher weder im Inland noch im Ausland in gleicher oder ähnlicher Form einer anderen Prüfungsbehörde vorgelegt.

Die Vorbereitung der Objektträger und sämtliche Färbungen an Präparaten wurden von mir selbstständig durchgeführt.

Die Gefrierschnitte der Präparate wurden durch die medizinisch-technischen Assistenten Nadine Hemstedt und Witali Lorenz durchgeführt.

Die PCR-Tests und Sanger-Sequenzierungen sind nach entsprechender Anleitung durch Frau Yvonne Kahlert und Herrn Dr. Justus Ackermann von mir selbst ausgeführt wurden.

Die Laser-Mikrodissektion wurde mit dem Leica LMD700 Laser Capture Microdissection System und der Leica LMD Software in der Imaging Facility im CECAD von mir selbstständig durchgeführt.

Die Identifizierung von Zellen während der Laser-Mikrodissektion erfolgte anfänglich mit Unterstützung von Frau Dr. Heike Göbel aus dem Institut für Pathologie Köln.

Die DNA-Isolation und die Whole-Genome Amplifizierung wurden von mir selbstständig durchgeführt.

Die Library Construction und das Whole-Genome Sequencing wurden von dem Cologne Center for Genomic (CCG) durchgeführt.

Der dieser Arbeit zugrunde liegenden Erhebung der Sequenzierungsdaten wurde ohne meine Mitarbeit in der Klinik für pädiatrischen Onkologie im Labor für Experimentelle Kinderonkologie von Herrn Dr. Christoph Bartenhagen durchgeführt.

Erklärung zur guten wissenschaftlichen Praxis:

Ich erkläre hiermit, dass ich die Ordnung zur Sicherung guter wissenschaftlicher Praxis und zum Umgang mit wissenschaftlichem Fehlverhalten (Amtliche Mitteilung der Universität zu Köln AM 132/2020) der Universität zu Köln gelesen habe und verpflichte mich hiermit, die dort genannten Vorgaben bei allen wissenschaftlichen Tätigkeiten zu beachten und umzusetzen.

Köln, den 26.02.2024

Unterschrift: 

Danksagung

Mein besonderer Dank gilt den Patienten und Eltern, die die in diesem Forschungsprojekt analysierten Tumorproben zur Verfügung gestellt haben.

Ich danke Herrn Prof. Dr. Matthias Fischer, meinem Doktorvater, für die Festlegung und Betreuung dieses Forschungsprojektes. Ich bin dankbar für die außerordentlich aufmerksame Unterstützung, kritische Auseinandersetzung und zahlreichen lehrreichen Gesprächen. Ich habe von seinem enormen Erfahrungs- und Wissensschatz lernen dürfen und wurde Teil eines herausragenden Forschungsumfeldes.

Ferner danke ich Herrn Dr. Justus Ackermann, meinem Zweitbetreuer. Ich bedanke mich für die praktische Einführung in die experimentelle Forschung, die umfangreichen Ratschläge und das Korrekturlesen dieser Dissertation.

Auch möchte ich meinen Kollegen des Labors und dem gesamten Team der experimentellen pädiatrischen Onkologie meinen Dank aussprechen, die mich durch ihr herzliches Willkommen heißen und ihren vielfältigen Bemühungen geprägt haben.

Ich möchte meinen großen Dank an die Studienstiftung des deutschen Volkes aussprechen, die mich sowohl finanziell als auch ideell unterstützt haben.

Des Weiteren möchte ich meinen Freunden und meiner entfernten Familie für ihre Geduld und stetige Motivation in den vergangenen Jahren danken.

Meinen Eltern und meinen Geschwistern danke ich besonders für ihre unerlässliche Unterstützung, kontinuierliche Ermutigung und großes Verständnis während der Arbeit an dieser Dissertation.

Gewidmet Kindern mit Neuroblastom.

Gewidmet meinen Eltern und Geschwistern.

Table of Content

List of abbreviations

ALT	Alternative Lengthening of Telomeres
APB	ALT associated PML bodies
bp	Base pairs
d	Days
DMSO	Dimethylsulfoxide
Dx	Diagnosis
FFPE	Formalin Fixed and Paraffin Embedded
GNBn	Ganglioneuroblastoma, nodular subtype
GC	Ganglionic cells
H&E	Haematoxylin and Eosin
INPC	International Neuroblastoma Pathology Committee Grading System
LCM	Laser Capture Microdissection
MAP2K7	Dual specificity mitogen-activated protein kinase kinase 7
NB	Neuroblasts
NTC	No Template Control
NX	Nextera Kit
PBS	Phosphate-buffered saline
pNT	Peripheral Neuroblastic Tumor
TERT	Telomerase reverse transcriptase
Tm	Annealing temperature
TMM	Telomere Maintenance Mechanism

1. Abstract

1.1. Abstract

Ganglioneuroblastoma, nodular subtype, (GNBn) is a rare, pediatric, peripheral Neuroblastic Tumor (pNT) of the sympathetic nervous system with mostly poor clinical outcome. Two thirds of Ganglioneuroblastoma, nodular subtype, are classified into the unfavorable subset.

This childhood malignancy is characterized as a composite tumor with two different histological components: the ganglioneuromatous and the neuroblastic component. It has remained uncertain, however, whether tumor cells of these two components are clonally related. In addition, it is still unclear which factors enable terminal differentiation in parts of the tumor, whereas other parts stay in a poorly differentiated state. GNBn is significantly heterogenous in outcome and its biology remains elusive, making further characterization of this entity necessary.

In this study, we have established a protocol to characterize neuroblasts and ganglionic cells individually using Laser Capture Microdissection. DNA of microdissected neuroblasts and ganglionic cells of 5 GNBn tumor samples in stage 4 was extracted and whole-genome sequenced. Mutations were called and subsequently validated through dideoxy-sequencing. Neuroblasts and ganglionic cells shared several mutations, while only selected mutations occurred in either cell type. In one case, biallelic inactivation of *MAP2K7* was found in neuroblasts, while ganglionic cells harbored a heterozygous mutation of *MAP2K7* only. Five additional neuroblastic tumors with a biallelic inactivation of *MAP2K7* were identified in our neuroblastoma sequencing data base. All six tumors lacked other frequent alterations of neuroblastoma, i.e., *MYCN* amplification, *ATRX* mutation, or *TERT* rearrangement.

The study demonstrated that ganglionic and neuroblastic cells are clonally related, as they shared several mutations. We also found evidence, however, that neuroblasts harbor private genomic alterations, such as inactivating mutations of *MAP2K7* and *ATRX*, which may account for the malignant properties of this cell type and their inability to differentiate in stage 4 GNBn. By contrast, malignant neuroblasts may differentiate into senescent ganglionic cells in the absence of such mutations.

1.2. Zusammenfassung

Das noduläre Ganglioneuroblastom (GNBn), ist ein seltener, kindlicher, peripherer neuroblastischer Tumor des sympathischen Nervensystems mit schlechtem klinischem Verlauf. Zwei Drittel der nodulären Ganglioneuroblastome werden in die ungünstige Subgruppe klassifiziert.

Dieser maligne Tumor im Kindesalter wird als zusammengesetzter Tumor mit zwei klonal unabhängigen Zellpopulationen betrachtet: eine ganglioneurmatöse und eine neuroblastische Population. Andere Studien deuten jedoch daraufhin, dass eine genetische Verwandtschaft zwischen beiden Zellpopulationen besteht. Das GNBn hat ein heterogenes, klinisches Outcome und die Biologie des Tumors ist bis heute nicht geklärt. Daher ist eine weitere Charakterisierung des Tumors notwendig.

In dieser Studie haben wir ein Protokoll entwickelt, um Neuroblasten und Ganglienzellen nach Mikrodissektion individuell zu charakterisieren. Die DNA von mikrodissezierten Neuroblasten und Ganglienzellen von fünf GNBn Tumoren im Stadium 4 wurde extrahiert und whole-genome-sequenziert. Die dadurch detektierten Mutationen wurden mittels Dideoxy-Sequenzieung validiert. Neuroblasten und Ganglienzellen zeigten mehrheitlich identische Mutationen und nur vereinzelt exklusive Mutationen. In einem Tumor wurde eine biallelische Inaktivierung von *MAP2K7* in Neuroblasten gefunden, wohingegen die Ganglienzellen lediglich eine heterozygote Mutation aufzeigten. Fünf weitere neuroblastische Tumore mit biallelischer Inaktivierung von *MAP2K7* wurden in unserer Neuroblastoma Datenbank gefunden. Diese insgesamt sechs pädiatrischen Patienten wiesen keine Neuroblastom-typischen genetischen Veränderungen auf: *MYC-N* Amplifikation, *ATRX* Mutation, *TERT* rearrangement.

Unsere Ergebnisse deuten darauf hin, dass Ganglienzellen und Neuroblasten klonal verwandt sind, da sie ein ähnliches Mutationsprofil aufweisen. Das exklusive Auftreten einer Inaktivierung von *MAP2K7* und *ATRX* in Neuroblasten unterstützt die Annahme, dass diese Mutationen für die malignen Eigenschaften und die fehlende Zelldifferenzierung von Neuroblasten in GBNn Tumoren Stadium 4 führend sind. Fehlen diese Mutationen, scheinen maligne Neuroblasten in seneszente Ganglienzellen zu differenzieren.

2. Introduction

2.1. Neural Crest Cells

The sympathetic nervous system arises from the neural crest, a cluster of cells from the neuroectoderm in early embryonal development. Cells of the neural crest are multipotent progenitor cells with the ability to differentiate into various cell types. Differentiation into the diverse cell types depends on activation of complex signaling pathways and transcription factors. Phox2b is one transcription factor that favors the neurogenesis of neuroblasts. These neuroblasts then develop into ganglionic cells (**Figure 1**). Malignant transformation however occurs once the maturation and differentiation processes are disrupted [1,2].

Schwann cells are non-neuronal, neuroglial cells that protect the neurons of the peripheral nervous system. Schwann cells exhibit remarkable plasticity and contribute to neural regeneration and immunological processes [3].

Schwann cells and neuroblasts share neural crest origin and interact with one another through neurotrophic factors. However, the impact of Schwann cells on neuroblastic tumorigenesis remains elusive [3]. Previous studies have suggested that Schwann cells may inhibit tumor angiogenesis, leading to an anti-tumor environment. These findings are supported by the fact that the mostly benign ganglioneuromatous tissue in ganglioneuroma or ganglioneuroblastoma is stroma/Schwann cell rich [4,5].

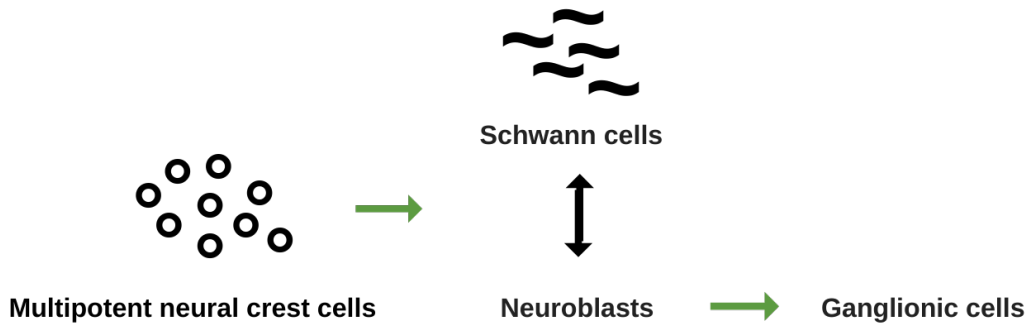

Figure 1 Neural crest cell maturation

Both Schwann cells and neuroblasts develop from the neural crest. Schwann cells and neuroblasts interact with each other through neutrophic factors. Neuroblasts can differentiate into ganglionic cells.

2.2. Neuroblastoma

Neuroblastic tumors are known for their biological and clinical heterogeneity.

Neuroblastic tumors are classified according to biological and clinical markers. Staging is a classification system that represents the progression of the tumor within the body (after surgery). In short, stage 1 refers to a localized tumor that has been removed completely with surgery. Stage 2A refers to an on-site tumor that could not be removed completely. Stage 2B additionally refers to spreading of the tumor to adjacent lymph nodes. Stage 3 additionally refers to tumors that are crossing the midline of the body. Stage 4 refers to tumors that have spread to distant sites. Stage 4S is a special stage that refers to children younger than 1 year old with metastases to liver, bone marrow, or skin [6].

Neuroblastic tumors are also classified into distinct histological groups. The International Neuroblastoma Pathology Classification differentiates four entities:

- Neuroblastoma
- Ganglioneuroblastoma, intermixed
- Ganglioneuroblastoma, nodular subtype
- Ganglioneuroma

The histological subtype neuroblastoma occurs most frequently and constitutes over two thirds of neuroblastic tumors.

In addition, neuroblastic tumors can be divided into various risk groups, according to the presence or absence of a number of clinical or molecular markers. The clinical courses range from spontaneous regression (low-risk neuroblastoma) to aggressive progression (high-risk neuroblastoma). In recent years, several studies shed light on the biology and tumorigenesis of neuroblastoma [7].

2.2.1. Telomere Maintenance Mechanisms

The malignant transformation of cells and subsequent tumorigenesis depend on a set of certain hallmarks, i.e., angiogenesis or the escape of transformed cells from the immune system [8]. One crucial hallmark is the activation of telomere maintenance mechanisms (TMM) to prevent permanent cell cycle arrest or apoptosis.

Telomeres are repetitive DNA and protein sequences at the ends of the chromosomes. They protect the DNA from being recognized as free double stranded DNA by the DNA damage response machineries, which may trigger cellular senescence or apoptosis. The maintenance of telomeres is thus vital for unlimited proliferation capacity and, hence, immortalization of tumor cells.

In most cases, telomere lengthening is conferred by induction of telomerase. Telomerase is a ribonucleoprotein made up of the catalytic subunit telomerase reverse transcriptase (TERT) and the RNA subunit TERC that is used as template to synthesize telomeres at the 3' end of the chromosome.

Expression of telomerase is restricted to cells and tissues with replicative functions, i.e., stem cells, bone marrow cells or germline cells. In normal cells, telomerase is silenced, and telomere shortening is an ageing related, physiological process that occurs with each DNA replication.

Cancer cells acquire alterations that activate telomere maintenance mechanisms (TMM). Alterations leading to telomerase induction are diverse, and may include amplification or rearrangement of the *TERT* gene, *TERT* promoter mutations, or activation of transcription factors that induce *TERT* expression, such as c-Myc. Telomerase reactivation as TMM occurs in over 80% of human cancer [9].

Another TMM is the Alternative Lengthening of Telomeres (ALT) pathway that is based on homologous recombination [9]. ALT as TMM occurs in over 10% of human tumors. One characteristic of cells undergoing ALT is the presence of extrachromosomal DNA that can be detected as ALT associated nuclear PML bodies (APB). Another characteristic of ALT-positive cancer cells is the heterogenous size of their telomeres. Both Telomere Maintenance Mechanisms, ALT and telomerase activation, may occur simultaneously within a tumor or even within a malignant cell. Mutations in the *ATRX* gene, encoding for chromatin remodeling proteins at telomeric regions, have been linked to ALT activation [9,10].

The activation of telomere maintenance mechanisms is a key hallmark of high-risk neuroblastoma [11,12]. In most of these tumors, telomere maintenance is conferred by induction

of telomerase, either through amplification of *MYCN* or genomic rearrangement of *TERT*. The remaining high-risk cases are ALT-positive, with roughly half of these bearing inactivating mutations of *ATRX*. By contrast, telomere maintenance mechanisms are invariably absent in low-risk neuroblastoma, which may result into spontaneous regression or differentiation in these tumors [11].

2.3. Ganglioneuroblastoma, nodular subtype

Ganglioneuroblastoma, nodular subtype, comprises 10% of neuroblastic tumors and is characterized by its specific histology.

According to the International Neuroblastoma Pathology Classification (INPC), ganglioneuroblastoma, nodular subtype, is characterized by at least one macroscopic visible neuroblastic nodule (stroma-poor) surrounded by more than 50% of ganglioneuroma (stroma-dominant) or ganglioneuroblastoma, intermixed (stroma-rich). On a microscopical level, there is a clear distinction between the neuroblastic nodule and the ganglioneuromatous component (**Figure 2**). GNBn has therefore been considered as a composite tumor, suggesting that the ganglioneuromatous component may arise from different clones than the neuroblastic component[13]. However, other studies have provided evidence for a common genetic origin of both tumor components [14].

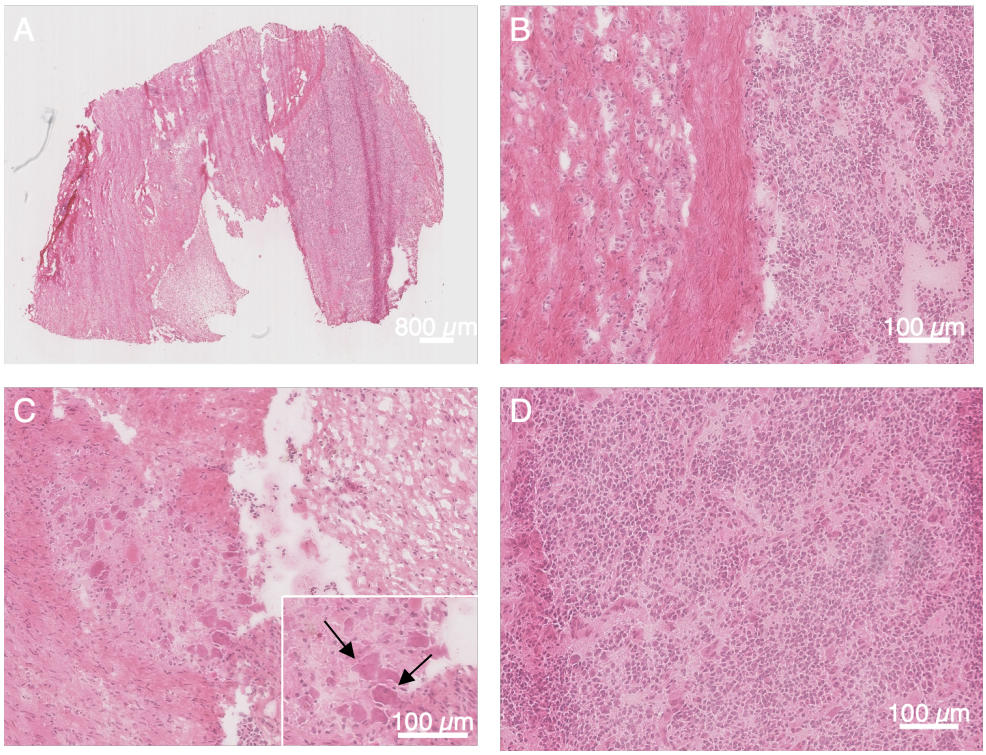

Figure 2 Histology of Ganglioneuroblastoma, nodular subtype

(**A**) Overview of a ganglioneuroblastoma, nodular subtype section. (**B**) Line of demarcation with ganglioneuromatous site on the left and neuroblastoma on the right side. (**C**) Ganglioneuromatous site with multiple ganglionic cells. (**D**) Neuroblastoma site with pathognomonic small blue round cells.

Ganglioneuroblastoma, nodular subtype, differs clinically from other neuroblastic tumors: Children with Ganglioneuroblastoma, nodular subtype (GNBn) are usually older than those with neuroblastoma. The majority of ganglioneuroblastoma, nodular subtype, tumors are classified as stage 4 disease, and the outcome of patients with GNBn is predominantly poor.

Regarding the biological features of GNBn, the *MYCN* oncogene, a biological risk factor highly prevalent in neuroblastoma, is rarely amplified [15,16]. Other biological and clinical prognostic risk factors such as grade of differentiation, initial treatment and stage that occur in neuroblastoma can also be found in ganglioneuroblastoma, nodular subtype [13,15].

According to the INPC, neuroblastic tumors are assigned to an either favorable or unfavorable prognostic subset, based on an age-linked evaluation of morphological indicators, i.e., the grade of differentiation and the Mitosis Karyorrhexis Index. The Mitosis Karyorrhexis Index measures the amount of cells in mitosis and karyorrhexis, meaning the fragmentation of the nucleus, per 5000 cells [17]. Initially, every ganglioneuroblastoma, nodular subtype, was categorized into the unfavorable histology group. Later it was observed that the nodular component in GNBn has not always been aggressive [18].

Thus, the INPC system was revised: Ganglioneuroblastoma, nodular subtype, can be divided into two prognostically distinct subsets, the clinical fate of which is determined by the neuroblastic component. Prognostic factors of the neuroblastic component are evaluated analogous to those in neuroblastoma. Accordingly, the two subtypes of GNBn have a significantly distinct survival: The overall survival rate is 90.5% for the favorable subset and 33.2% for the unfavorable subset [18,19].
In total, two thirds of ganglioneuroblastoma, nodular subtype, are classified into the unfavorable subset [19].

The tumor site of ganglioneuroblastoma, nodular subtype, is mainly adrenal, abdominal and thoracic. The most common metastatic sites include bone marrow and bone. No gender difference was identified. Common initial symptoms of patients with ganglioneuroblastoma, nodular subtype, are abdominal pain, abdominal swelling and fever [15,20].

One study gives evidence against separate clonal origin of the neuroblastomous and ganglioneuromatous component, proposing that the aggressive behavior of Ganglioneuroblastoma, nodular subtype, cannot solemnly be explained by the existence of distinct clones [14]. However, there is also evidence for two distinct clones within Ganglioneuroblastoma, nodular subtype and even within Neuroblastoma itself, speaking for high biological variance and suggesting a case-by-case approach [21,22].

2.4. Aims of the study

The aim of this study was to determine the mutation profile and clonal relationship of ganglionic and neuroblastic cells occurring in GNBn.

First, we hypothesize that neuroblasts and ganglionic cells are derived from common precursors and thus clonally related.

Second, we hypothesize that neuroblasts harbor somatic alterations that inhibit terminal differentiation and facilitate infinite growth and dissemination, whereas such alterations are lacking in ganglionic tumor cells.

Third, we hypothesize that our approach will enable the identification of relevant genetic alterations that drive malignant progression from benign ganglioneuroma to unfavorable neuroblastoma, thereby providing novel insights into the molecular pathogenesis of this deadly pediatric malignancy.

2.5. Workflow

To test these hypotheses, I isolated clusters of the distinct cell types by Laser Capture Microdissection and determined genomic alterations by whole-genome sequencing. Somatic mutations of interest were validated by dideoxy-sequencing (**Figure 3**).

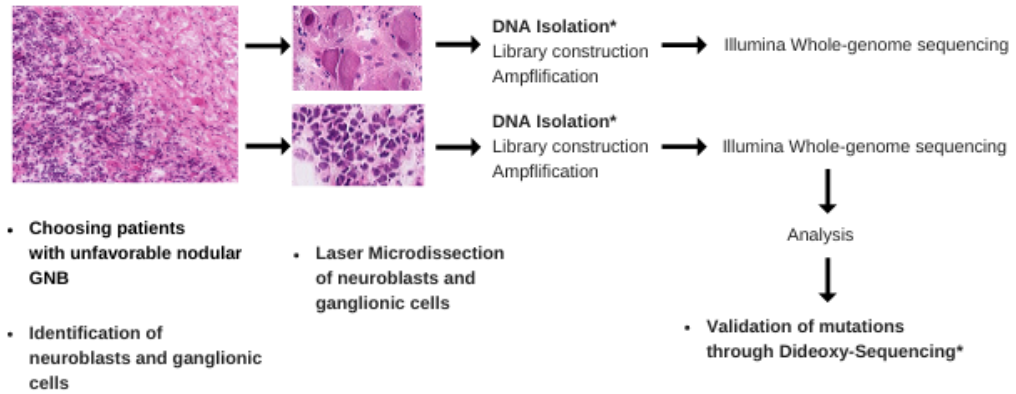

Figure 3 Workflow of the study

To determine the mutational profile of preselected GNBn, both neuroblasts and ganglionic cells were microdissected individually with a subsequent extraction of DNA and whole-genome sequencing. The mutations found were validated through dideoxy-sequencing.

3. Material und Methods

3.1. Selection of patients

Patients were selected from the biobank of the national neuroblastoma register at the Department of Pediatric Oncology and Hematology of the University Children's Hospital Clinics of Cologne. These Patients had been registered and treated according to the trials NB97 or NB2004 of the Gesellschaft für Pädiatrische Onkologie (GPOH). Collection and use of specimens was approved by the Institutional Review Board of the Medical Faculty, University of Cologne (9764 for NB97 and 04-049 for NB2004), and informed consent was obtained from all patients or their guardians.

A database query was performed with the following requirements:

- The tumor had to be diagnosed as ganglioneuroblastoma, nodular subtype, using the International Neuroblastoma Pathology Committee Grading System [23].
- The disease had to be categorized as stage 4 with unfavorable clinical course. Unfavorable clinical course in this context refers to progression of the tumor, relapse of the disease, or death of the patient.
- Fresh frozen tissue samples of the tumors had to be available.

Twenty-one cases met these requirements. However, in addition to these requirements, the tumor samples needed to cover the histological features of our interest, i.e., both poorly differentiated neuroblastic cells and stroma-rich areas with several intact mature ganglionic cells had to be present within individual sections. Lastly, matched normal control samples (i.e., blood) had to be available from all samples to ensure accurate calling of somatic mutations. If normal control samples were not available, the tumor section needed to have normal tissue that could be microdissected and analyzed alternatively.

Taken all these requirements into account, a total of five cases were suitable for the subsequent analysis. The five cases covered an age range of approximately three to ten years, including four males and one female (**Table 1**).

Table 1 Clinical features of GNBn cohort

Abbreviations: d = days, Dx = diagnosis, EFS = Event-Free Survival, OS = Overall Survival.

Case	Histology	Stage	MYC-N	Age in d at Dx	Event	EFS	Survival	OS
GNBn_1	GNBn	4	1	3672	Relapse	2105	No	2828
GNBn_2	GNBn	4	1.5	2095	Relapse	637	Yes	5538
GNBn_3	GNBn	4	1.5	1034	Relapse	1683	No	2662
GNBn_4	GNBn	4	1	1606	Relapse	1818	Yes	1819
GNBn_5	GNBn	4	1	1969	Progress	91	No	636

3.2. Preparation of slides

Laser Capture Microdissection (LCM) was performed on the same day as slides from Fresh Frozen tissue were prepared and stained according to a modified haematoxylin/eosin (H&E) protocol [24].

To avoid DNA contamination, cuvettes were sprayed with DNA-ExitusPlus Spray (Applichem) and rinsed with Nuclease Free Water (MerckMillipore) right before usage.

The fresh frozen tissues were stored at -80°C. The knife of the cryostat was cleansed with 100% ethanol to eliminate contaminants. Tissue sections of 7 µm were cut using a cryostat. This section thickness was chosen to cover the relatively large nuclei of ganglionic cells by laser microdissection on the one hand, and to guarantee sufficient histological assessment on the other hand. The sections were then mounted on membrane slides (MembraneSlide 1.0 PEN, Carl Zeiss MicroImaging). The slides were not covered with a coverslip to allow dissected cells and tissue to fall into collecting caps. The membrane slides were exposed to 254 nm UV light for 30 minutes and stored at room temperature prior to cutting frozen sections. UV radiation was performed to enable further elimination of contaminating nucleic acids and nucleases and to improve the mounting of slides [24].

After sections had been prepared and air-dried for 2 minutes at room temperature H&E staining was performed following the protocol indicated in **Table 2**:

Table 2 H&E staining protocol

Abbreviations: RT = Room Temperature, mins = minutes, secs = seconds.

Step	Reagent	Temperature	Time
1 Fixation	70% Ethanol	-20°C	1 min
2 Washing	Tap Water	RT	Dip ~ 5x
3 Stain	Hematoxylin	RT	2 mins
4 Bluing	Tap Water	RT	2 mins
5 Stain	Eosin	RT	15 secs
6 Fixation	70% Ethanol	RT	Dip ~ 3x
7 Fixation	95% Ethanol	RT	Dip ~ 3x
8 Fixation	100% Ethanol	RT	Dip ~3x
9 Drying		RT	~ 2 mins
10 Covering	Liquid Cover Glass	RT	3 pumps

The H&E staining protocol contained a fixation step of 2 minutes with -20°C cold 70% ethanol, washing of the ethanol by dipping the slides in tap water until slides were clear, which equals to a dipping of about five times, a staining step with haematoxylin for 2 minutes, another 2 minutes of dipping the slides into regular tap water that was used as bluing reagent, and a counterstaining step with eosin for 15 seconds. This staining step was followed by a fixation step of ascending ethanol series of 70%, 95% and 100% ethanol by dipping the slides three times into the solutions. The slides were airdried for about 2 minutes at room temperature. The slides were then sprayed with the Liquid Cover Glass (Carl Zeiss Microimaging) by using three pumps at a distance of 10 cm from the slides.

The Alcohol reagents had been prepared by using distilled water and 100% ethanol. Hemalum solution acid acc. to Mayer (Carl Roth) and Eosin Y-Solution 1% in water (Carl Roth) were used as dyes.

3.3. Identification of cells and Laser Capture Microdissection

Neuroblasts and ganglionic cells are distinct in their morphological appearance and can therefore be identified without additional immunohistochemical staining.

The microdissection was performed using the Leica LMD700 Laser Capture Microdissection System including the Leica LMD Software V8.1 at the Imaging Facility at the Excellence Cluster CECAD Cologne. Microdissection is an established technique (**Figure 4**), which allows collection of specific cells or tissue of interest by applying a high laser power to the specimen [25].

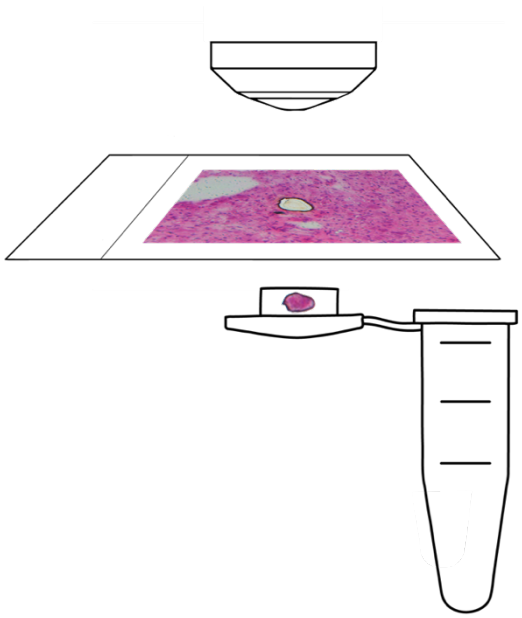

Figure 4 The Laser Capture Microdissection technique

The laser cuts through the section. The dissected tissue then falls into a collecting tube.

The settings for the laser microscope were tested and calibrated at every session on the software, in order to guarantee that the laser power and aperture are high enough to dissect through the tissue thoroughly (**Table 3**). A safe distance of the laser from the cell nucleus was kept to prevent potential damage. It had to be ensured that the safe distance was narrow enough to specifically target cells of interest and to thus avoid contamination of unwanted cells.

Table 3 Settings for the Laser

Magnification	10x	20x	40x
Power	17	30	28
Aperture	20	1	1
Speed	7	5	10

Once settings were established, cells of interest were selected and dissected by the laser. The cells then fell into the collecting caps, which were 0.2 ml PCR tubes with separate 8-strips flat caps (ZEISS Microscopy). In contrast to regular 0.2 ml PCR tubes, we found that the unattached 8-strips caps were the easiest to handle when placing and removing the caps on and off the Microscope and for the succeeding DNA isolation.

After microdissection, we inspected the caps through the Laser Microscope to make sure the cells of our interest were successfully captured.

About four to seven slides with two sections per slide were prepared for each tumor. Neuroblasts were microdissected in areas of 40.000 µm². An area of 160 µm² contains about one cell. Thus, a minimum of at least 250 neuroblasts were isolated for every case. Ganglionic cells were microdissected separately, with a minimum of 20 cells per sample. Additionally, areas of 3x 40.000 µm² of normal cells were microdissected for case GNB_1, because blood samples, the equivalent to normal cells, were not available for this case.

An experienced pathologist from the Institute for Pathology of Cologne assisted the microdissection process to ensure selection of correct cell types.

3.4. DNA Isolation

DNA Isolation was performed with the QIAamp DNA Micro Kit (Qiagen) according to the manufacturer's protocol immediately after microdissection.

Once the caps had been removed from the microscope, proteinase K and buffer ATL from the kit were added to the rim of the cap while making sure that no solution was being soaked back into the pipette when removing the pipette from the cap. The cells were incubated at 56°C for 3 hours in a 1.5 ml tube in a water bath or a Thermocycler. Carrier RNA, as proposed by the manufacturer for small input DNA, had not been used. The DNA was eluted in 20 µl buffer. Isolated DNA samples were stored at 4°C until further processing.

3.5. Different methods of Genomic Library construction

Generation of genomic libraries and sequencing was performed by the Cologne Center for Genomics (CCG).

We tested three different methods to construct genomic libraries (**Figure 5**).

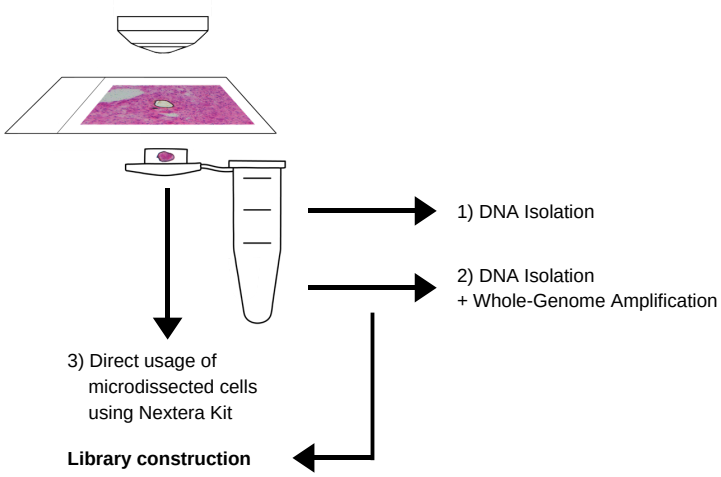

Figure 5 Three different methods for genomic library construction

The microdissected cells were processed in 3 different ways for constructing a genomic library.

1) The DNA was isolated from the microdissected tissue.
2) The isolated DNA of the microdissected tissue was whole-genome amplified to increase DNA yield for genomic library construction.
3) The microdissected tissue was processed directly with the Nextera Kit without prior DNA isolation.

3.5.1. Method 1: DNA Isolation

In a first attempt, the DNA from the microdissected tissue was isolated using the QIAamp DNA Micro Kit (Qiagen) according to the manufacturer's protocol. This DNA was then used for library construction using the QIAseq Ultralow Input Library Kit.

3.5.2. Method 2: DNA Isolation and Whole Genome Amplification

In a second attempt, the isolated DNA that had been extracted using the QIAamp DNA Micro Kit (Qiagen) was subsequently whole-genome amplified using the REPLI-g Single Cell Kit (Qiagen) to increase DNA yield for library preparation.

3.5.3. Method 3: Direct Usage of Microdissected cells using Nextera Kit

In a third attempt, the microdissected tissue was used directly for library construction, i.e., without isolating the DNA, using the Nextera DNA Flex Library Prep Kit. The kit uses tagmentation, a step in which DNA is fragmented and tagged to adapter sequences by a transposase, and enzymatic reactions to fragment the DNA.

3.6. Final Method of Genomic Library Construction and Whole-Genome Sequencing

After evaluation of the three approaches, we used method 1 for further experiments. The isolated DNA was checked for quality prior to library construction using the Agilent 2200 TapeStation with the Genomic DNA ScreenTape assay. Its software assesses DNA quantity by electrophoresis and DNA integrity by generating a DNA Integrity Number. The DNA Integrity Number is equivalent to the degree of degradation [26].

High Molecular DNA was fragmented prior to library construction using the QIAamp UltraLow Input Library Kit. Fragmentation method should be chosen cautiously, since excessively fragmented DNA may be insufficient in size for sequencing. DNA was fragmented to a size of roughly 400 bp by a physical method using Bioruptor (Bioruptor®) in 0.1 ml microtubes for DNA shearing. The sonication was performed at 4°C in a final volume of 45 µl and seven cycles, except for case GNBn_1 that was fragmented in nine cycles.

The QIAseq Ultralow Input Library Kit contains steps of end-polishing, ligation of adapters, cleanup and library amplification. The DNA was whole-genome amplified with 14-16 PCR cycles. An additional reaction cleanup and elimination of dimers was performed by size selection with a targeted insert size of 400 bp using Agencourt AMPure XP beads.

The quality, i.e., accurate size distribution of fragments and lack of adapter dimers, of each library was assessed using Agilent 2200 TapeStation with the D1000 ScreenTape assay, irrespective of the method of genomic library construction.

Whole-genome sequencing was performed on the Illumina NovaSeq 6000 instrument with 2*150 bp paired-end sequencing.

3.7. Analysis of sequencing data

To assess the initial read quality, sequencing data were analyzed using the software FastQC (https://www.bioinformatics.babraham.ac.uk/projects/fastqc/). The sequencing data were then aligned to the reference genome hg19/NCBI build 37 using BWA. After removing duplicates,

which may have occurred in previous amplification steps during library generation, the analysis proceeded with somatic mutation calling using an inhouse pipeline that detects single nucleotide variants, insertions and deletions, genomic rearrangements and copy number variations, as described previously [11]. Following the mutation calling, a manual inspection of variants was performed with IGV (Integrative Genomics Viewer, https://software.broadinstitute.org/software/igv/) to confirm and interpret genomic alterations.

3.8. Validation of mutations

To validate somatic mutations in neuroblasts, bulk tumor DNA of each tumor sample was used for PCR amplification of regions of interest and dideoxy-sequencing. To validate somatic mutations in ganglionic cells, isolated DNA from microdissected ganglionic cells of each tumor was first whole-genome amplified using the REPLI-g Single Cell Kit (Qiagen), followed by PCR amplification of regions of interest and dideoxy-sequencing. In case GNBn_4, one mutation (**Figure 17**) identified in neuroblasts was also validated by first whole-genome amplifying DNA from microdissected neuroblasts.

3.8.1. Whole genome amplification (WGA)

WGA was performed according to the manufacturer's protocol with no modifications using REPLI-g Single Cell Kit (Qiagen) for amplification of purified genomic DNA. 2.5 µl template DNA were used as starting volume. DNA yield of the WGA ranged from 200 to 500 ng/µl. The DNA was then diluted to 1:200, 1:100 or 1:50.

3.8.2. Polymerase Chain Reaction (PCR)

Primers were designed using the NCBI Primer Blast tool (https://www.ncbi.nlm.nih.gov/tools/primer-blast/) and ordered from ThermoFisher. The following primers were used for detecting alterations identified in tumors GNBn_1 and GNBn_2 (**Table 4**):

Table 4 Primers for amplification of gene fragments from tumors GNBn_1 and GNBn_2

Abbreviations: T_m, Annealing Temperature

Case	Gene	Sequence (5'->3') Forward	Sequence (5'->3') Reverse	T_m
GNBn_1	MAP2K7	CTCCTTCCCCCACACACATC	GGTGACTCAGTCTTCGCCAT	59°
	TOX2	ACTCTTCTCACTCGGGCAGA	CTGAGCCCAGGAAAGACCTC	58°
	GPR6	CTGGAGCTGTCCTCGCAG	CATGATGCCGAAGACCATGAA	59°
	GPR6	GCTGGAGAAAACGCGCTG	CATGATGCCGAAGACCATGAAG	59°
GNBn_2	ATRX	ATGAATGGAACAGAGAGGTAACAG	AAAATGAAGGGTTAGGCTGCTG	60.7°

The following primers were used for the MAP2K7 cohort (**Table 5**):

Table 5 Primers for amplification of MAP2K7 gene fragments

Abbreviations: T_m, Annealing Temperature

Case	Gene	Sequence (5'->3') Forward	Sequence (5'->3') Reverse	T_m
GNBn_1	MAP2K7	CTCCTTCCCCCACACACATC	GGTGACTCAGTCTTCGCCAT	59°
GNBn_1	MAP2K7.2	GGACTCACAGTTGCTCCCC	ATCCTTGAACCAGGACGCC	59°
M-GNBi_02	MAP2K7	TGTGAAGGCGCTGTACTACC	AACTCACCAACGAGATGCCC	67.7°
M-GNBn_03	MAP2K7	CCAGATCAAGCTCTGCGACT	GGGGCTCTTCCTGTAGGACT	56°
M-GNBi_04	MAP2K7	CTATGACATCCGGGCCGAC	CCATTCCCCTCCTGCCATTG	62°
M-NB_05	MAP2K7	CCAGATCAAGCTCTGCGACT	GGGGCTCTTCCTGTAGGACT	56°
M-NB_0606	MAP2K7	CTATGACATCCGGGCCGAC	CCATTCCCCTCCTGCCATTG	62°

Primers were dissolved to a concentration of 100 mM in TE Buffer (Invitrogen). The primers were then diluted to 10 mM stocks with nuclease-free water.

PCR was performed using the Q5 Polymerase Kit (New England Biolabs) and the following protocol ():

Reagent	**Volume in µl**
Q5 Reaction Buffer	5
10 mM dNTPs	0.5
Forward Primer (10 mM)	1.25
Reversed Primer (10 mM)	1.25
Template	Variable, i.e.,1
Q5 Enhancer	5
H20	Ad 25 µl
Q5 Polymerase	0.25
Total Reaction Volume	**25**

The following cycling conditions were used (**Table 6**):

Table 6 Thermocycler settings

Step	1	2	3	4	5	6	7
Time	00:30	00:10	00:30	00:30	38x	2:00	∞
Temperature	98°	98°	59°	72°		72°	10°

Amplification of *MAP2K7* fragments from ganglionic cells of case GNBn_1 required a more specific PCR as background noise was excessive within the chromatogram. Therefore, a semi-nested PCR was performed (see **Table 7**, **Table 8**).

Semi-nested PCR for amplification of *MAP2K7* fragments from ganglionic cells of case GNBn_1

First round of amplification:

For the first round of semi-nested PCR amplification, the primers MAP2K7_F1 and R1 were used.

Table 7 Semi-nested PCR protocol, first round

Component	**Volume in µl**
Q5 Reaction Buffer	5
10mM dNTPs	0.5
Forward Primer	0.5
Reversed Primer	0.5
Template	2 (DNA template concentration 3 ng/µl)
Q5 Enhancer	5
H20	11.25
Q5 Polymerase	0.25
Total Reaction Volume	**25**

Cycling conditions were as indicated in **Table 6**, with the exception that 30 cycles of amplification were performed (step 5 in **Table 6**).

Second round of amplification

For the second round of semi-nested PCR amplification, the primers MAP2K7_F1 and R2 were used.

Table 8 Semi-nested PCR protocol, second round

Component	Volume in µl
Q5 Reaction Buffer	5
10 mM dNTPs	0.5
Forward Primer	0.5
Reversed Primer	0.5
Template	2 (DNA template concentration 0.9ng/µl)
Q5 Enhancer	5
H20	11.25
Q5 Polymerase	0.25
Total Reaction Volume	**25**

Cycling conditions were as indicated in **Table 6**, with the exception that 28 cycles of amplification were performed (step 5 in **Table 6**).

The DNA concentration was quantified with the Qubit dsDNA BR Assay Kit.

Following the PCR, a 1.5% agarose gel was prepared by dissolving 1.5 g agarose powder (Lonza SeaKem LE Agarose) in 150 ml TEA buffer (980 ml water + 20 ml TEA Buffer (Carl Roth Rotiphorese 50x TAE buffer). Subsequently, 6 µl of loading dye LD (iNtRON RedSafe Nucleic Acid Solution 20.000x) were added to the mix.

If PCR products visible on the gel were of the expected size, the product of the PCR reaction was directly sequenced by dideoxy-sequencing. If multiple PCR products were visible on the gel, the band with the expected base pair size was cut out and DNA extracted using the QIAquick Gel Extraction kit prior to dideoxy-sequencing.

3.9. Senescence staining

Senescence was examined using the abcam senescence detection kit ab65351 according to the manufacturer's protocol with minor modifications for fresh frozen slides:

The slides were encircled with a glass writing pen and fixed at room temperature for 15 minutes with the fixative solution of the kit that had been modified by adding 90 µl 1 N HCl to the solution, which resulted in a pH level of 5.88. The pH level at which the staining is performed is essential in the ß-Gal essay [27]: The lower the pH level, the more intense is the blue chromogen for optimal staining results.

The slides were washed by dipping the slides 4-10 times in PBS. Staining mix was then pipetted onto the sections of the slide. The staining mix was prepared by mixing 470 µl staining solution, 5 µl staining supplement and reconstituted 25 µl x-gal/DMSO. The total amount of 500 µl staining mix was enough solution for about 6 sections (around 80 µl per section). The slides were then placed in a wet chamber which was incubated overnight for at least 18 hours in an incubator at 37°C. The next day, the staining mix was washed off the sections with PBS. Afterwards, the sections on the slides were counterstained with Nuclear Fast Red for 1 minute and washed with distilled water. The wet slides were finally coverslipped with 1 drop of the mounting medium Aquatex®.

4. Results

4.1. Establishing a protocol to isolate distinct cell populations by microdissection

4.1.1. Microdissection of ganglionic cells and neuroblasts

The histology of tissues mounted on membrane slides appear different from the histology on covered slides [28]. The tissue appears to be blurrier and more indistinct (**Figure 6**). A notable improvement of the quality of histological sections was achieved by using the Liquid Cover Glass, which mimics a regular cover glass.

Staining eosin for 30 seconds turned out to be the optimal staining time to label individual cells, which is prerequisite for laser capture microdissection.

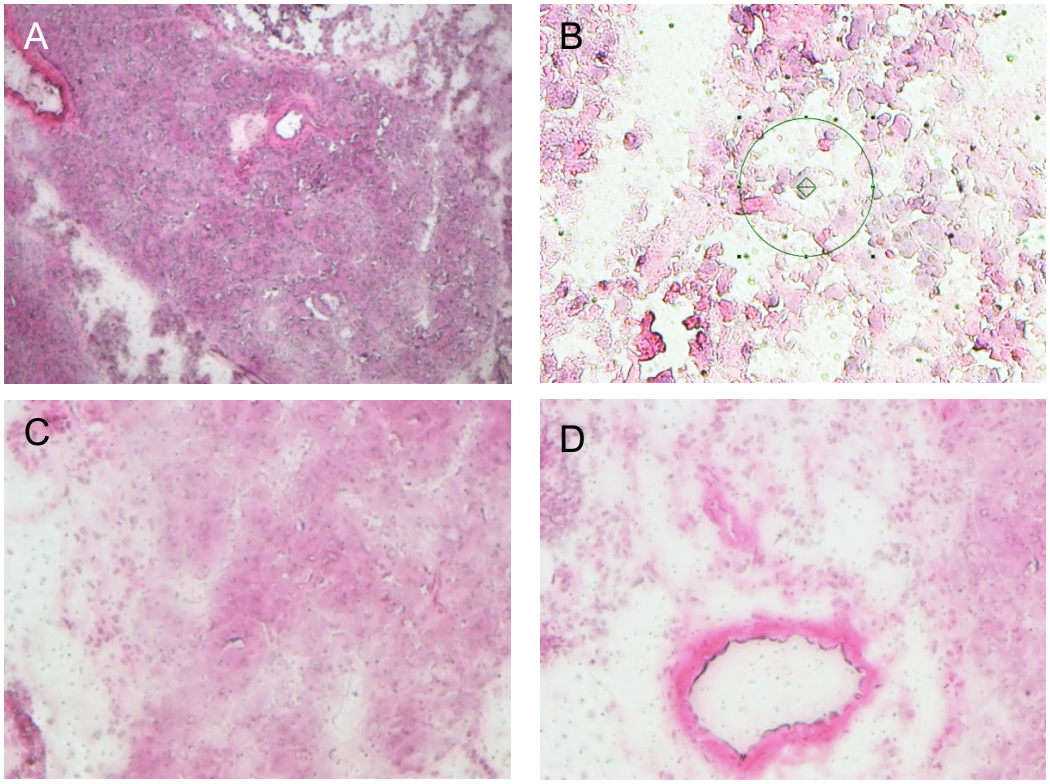

Figure 6 Histology of neuroblastoma with and without Liquid Cover Glass

Panels (**A**) and (**B**) show HE stained neuroblastoma sections of uncovered slides without the additional usage of Liquid Cover Glass. The upper left panel shows an overview of the sample section at 100x, the upper right panel magnification at 200x, with blurred tissue and clustered, indistinct cells. Panels (**C**) (100x) and (**D**) (200x) show the HE stained neuroblastoma with Liquid Cover Glass.

Ganglionic cells are relatively large compared to the rest of the cells occurring in GNBn sections. Ganglionic cells at various levels of maturation and differentiation may be present, and the diameter of the cells may thus range from about 15 µm to 30 µm.

We excluded intermediate or early levels of ganglionic cell differentiation by choosing mature ganglionic cells only, with a size of about 30 µm in diameter, and large marginal cell nuclei (**Figure 7**). The size of the cell and the marginal cell nucleus were our main decision criterion for microdissecting ganglionic cells. Some ganglionic cells had no visible nucleus (probably due to the section plane) and were subsequently not microdissected. Furthermore, we only microdissected ganglionic cells in the ganglioneuromatous, i.e., the stroma rich, component to avoid possible contamination with neuroblasts. Neuroblasts have the typical small blue round cell appearance and cluster densely (**Figure 8**), which facilitated identification of neuroblast areas for microdissection.

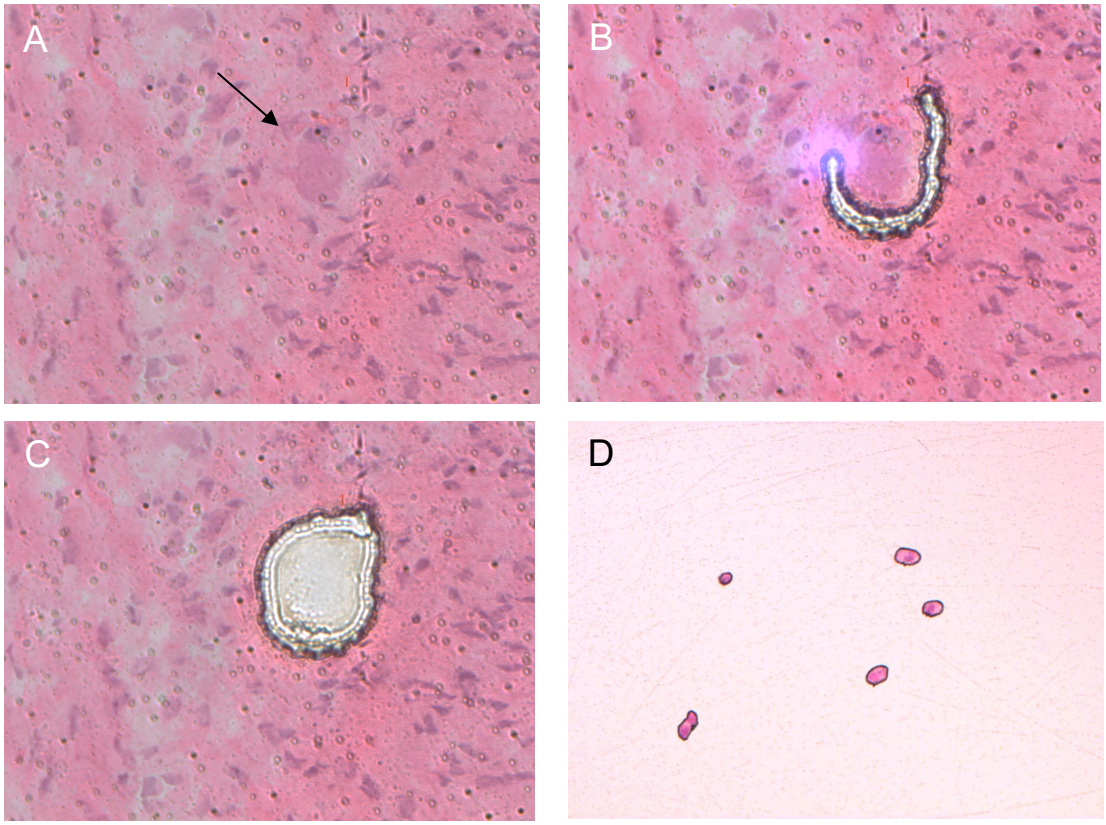

Figure 7 Microdissection of ganglionic cells

(**A**) Identification of a ganglionic cell by its large size with ample cytoplasm and a marginal cell nucleus (arrow). This cell can be classified as a ganglionic cell. (**B**) The ganglionic cell is being microdissected through laser application. (**C**) The ganglionic cell has been excised. (**D**) Five ganglionic cells in the collecting cap.

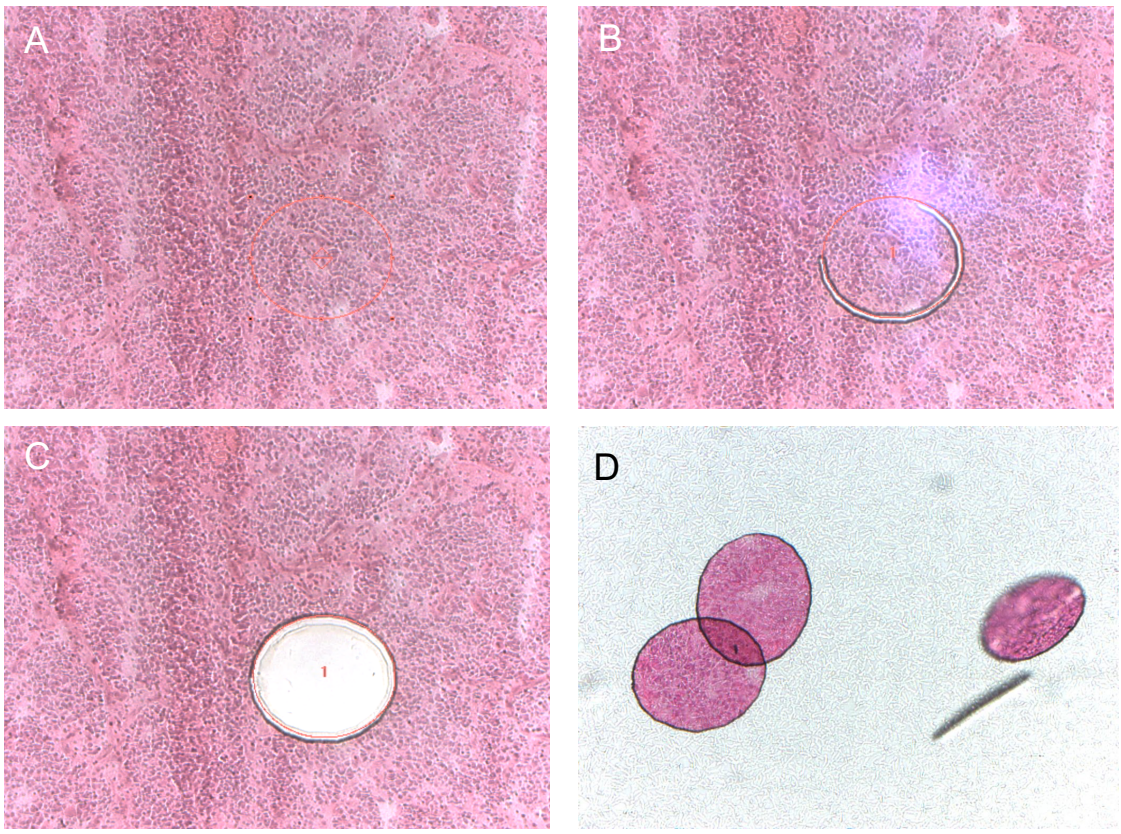

Figure 8 Microdissection of neuroblasts

(**A**) Densely clustered small blue round cells, corresponding to malignant neuroblasts of poorly differentiated neuroblastoma. (**B**) A cluster of neuroblasts is being microdissected. (**C**) The cluster of neuroblasts has been successfully excised. (**D**) Four clusters of neuroblasts in the collecting cap.

4.2. Establishing a protocol to isolate DNA from microdissected tissue

4.2.1. Test Run

A test run with a neuroblastoma sample tissue had been performed prior to using GNBn with the goal to determine the minimum number of microdissected cells needed to obtain sufficient DNA yield.

In this test run we excised areas of different sizes from the neuroblastoma test sample, corresponding to ranging from roughly 20 to 750 cells. We also assessed the impact of using samples multiple times for microdissection, with recurrent thawing and freezing. We found that DNA was detectable already in samples consisting of 20 cells only, although inconsistently and at very low concentrations (**Table 9**). By contrast, DNA was readily detectable in samples consisting of at least 500 cells. We also found that freshly prepared samples revealed higher and more consistent DNA yields than samples that had been thawed previously (**Table 10**).

Table 9 Test Run Library Check 1

Abbreviations: F = Freshly prepared sections that had been generated immediately before LCM usage, G = Frozen sections that had already been thawed, microdissected and restored prior to LCM usage.

Sample	Qubit High Sensitivity [ng/µl]	Concentration	Size [bp] before size selection	Estimated number of cells
F1_N	/	0.1 ng/µl	568	20
F2_N	/	/	666	20
G3_N	/	0.02 ng/µl	554	60
F4_N	/	/	656	70
G5_N	/	/	660	390
F6_N	/	2.3 ng/µl	640	500
F7_N	/	2.15 ng/µl	576	750

Table 10 Test Run Library Check 2

Abbreviations: F = Freshly prepared sections that had been generated immediately before LCM usage, G = Frozen sections that had already been thawed, microdissected and restored prior to LCM usage.

Sample	Qubit High Sensitivity [ng/µl]	Concentration	Size [bp] before size selection	Estimated number of cells
F_1	1.82 ng/µl	2.5 ng/µl	463	50
G_2	1.36 ng/µl	0.16 ng/µl	402	100
F_3	2.14 ng/µl	4.07 ng/µl	437	180
F_4	1.82 ng/µl	4.21 ng/µl	417	350
G_5	1.85 ng/µl	2.02 ng/µl	430	390

4.2.2. GNBn cohort

For the study, we selected five cases of GNBn, all of which were obtained from stage 4 patients older than 18 months at diagnosis, and thus classified as high-risk (see **Table 1**). All cases were non-*MYCN*-amplified.

DNA concentration after DNA isolation during Quality Check assessment with the TapeStation was already expected to be low. Ganglionic cells generally had a lower yield (**Table 11**) than neuroblasts (**Table 12**). The relatively high DNA concentration suggest a certain inaccuracy of cell numbers, DNA concentration, or both.

Table 11 DNA yield of ganglionic cells in TapeStation Quality Check

Case	GNBn_1	GNBn_2	GNBn_3	GNBn_4	GNBn_5
Cells	40	78	64	89	60
DNA yield	1.91 ng/µL	2.48 ng/µL	3.5 ng/µL	2.34 ng/µL	2.24 ng/µL

Table 12 DNA yield of neuroblasts in TapeStation Quality Check

Case	GNBn_1	GNBn_2	GNBn_3	GNBn_4	GNBn_5
Cells	2500	5250	5000	7000	7000
DNA yield	2.69 ng/µL	3.46 ng/µL	5.09 ng/µL	4.19 ng/µL	4.23 ng/µL

After processing the DNA samples with the QIAseq Ultralow Input Library Kit, the resulting libraries were assessed for quality by a Library Check (DNA concentration and fragment size) with the TapeStation (**Table 13**).

Table 13 Library Check of GNBn cohort

Abbreviations: NB = Neuroblasts, GC = Ganglionic cells, Normal = Non-malignant cells of the patient.

Sample	Qubit High Sensitivity [ng/µl]	Concentration before size selection [ng/µl]	Size [bp] before size selection	Microdissected area or number of cells
GNBn_1NB	2.69 ng/µl	32.7 ng/µl	428	10x 40.000 µm² = 2500
GNBn_1GC	3.82 ng/µl	32.1 ng/µl	431	40
GNBn_1Normal	Total DNA: 1.8 ng	32.7 ng/µl	496	3x 40.000 µm² (3 vessels)
GNBn_2NB	3.46 ng/µl	6.48 ng/µl	502	21x 40.000 µm² = 5250
GNBn_2GC	2.48 ng/µl	7.71 ng/µl	374	78
GNBn_2Normal	59 ng/µl	4.73 ng/µl	480	Blood
GNBn_3 NB	5.09 ng/µl	11.4 ng/µl	404	20x 40.000 µm² = 5000
GNBn_3GC	3.5 ng/µl	8.25 ng/µl	325	64
GNBn_3Normal	53.6 ng/µl	3.88 ng/µl	518	Blood
GNBn_4NB	4.19 ng/µl	14.2 ng/µl	529	28x 40.000 µm² = 7000
GNBn_4GZ	2.34 ng/µl	12.3 ng/µl	372	89
GNBn_4Normal	44.8 ng/µl	1.89 ng/µl	488	Blood
GNBn_5NB	4.23 ng/µl	3.09 ng/µl	541	28x 40.000 µm² = 7000
GNBn_5GZ	2.24 ng/µl	1.66 ng/µl	330	60
GNBn_5Normal	93.6 ng/µl	3.06 ng/µl	503	Blood

The size of the fragments of each library was crucial for deciding whether the libraries were suitable for 2x150 bp sequencing or not.

DNA of case GNBn_1 had been fragmented in nine cycles, which resulted in an optimal size of DNA fragments for sequencing: DNA of neuroblasts had a size of 428 bp, and DNA of ganglionic cells a size of 431 bp. When using the same number of cycles of fragmentation for DNA of cases GNBn_2-5, we noticed that the fragments were too small for the sequencing approach (data not shown). Consequently, we decided to reduce the number of cycles of fragmentation to seven.

Using the modified fragmentation approach, the average size of neuroblasts and ganglionic cells was about 300-400 bp (**Figure 9**, **Figure 10**, **Figure 11**), which was suitable for 2x150 bp sequencing.

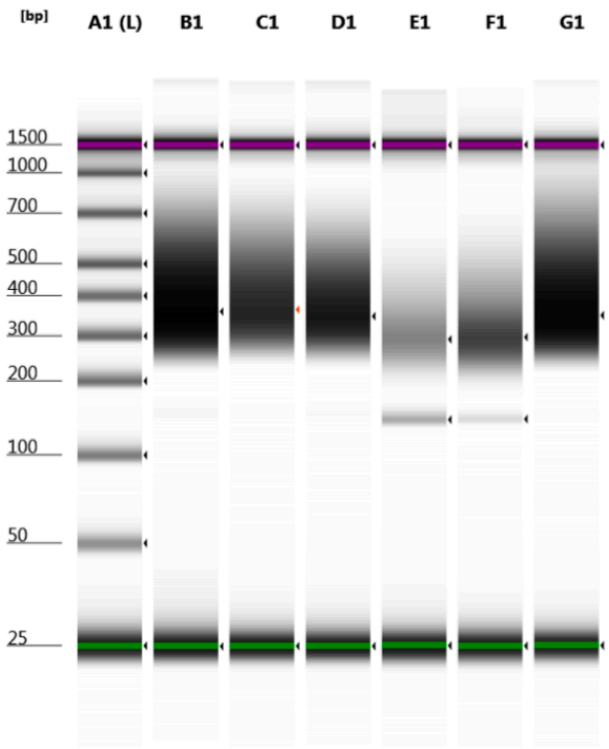

Figure 9 Library check results of neuroblasts and ganglionic cells of GNBn_1
(**B1**) Ganglionic cells. (**C1**) Neuroblasts. (**D1**) Neuroblasts. (**E1**) Neuroblasts. (**F1**) Ganglionic cells. (**G1**) Neuroblasts. Library check of DNA from ganglionic cells (**B1**) and neuroblasts (**G1**) assessed by electrophoresis using the Agilent 2200 TapeStation, showing fragment sizes of about 300-400 bp each, suitable for 2x150 bp sequencing.

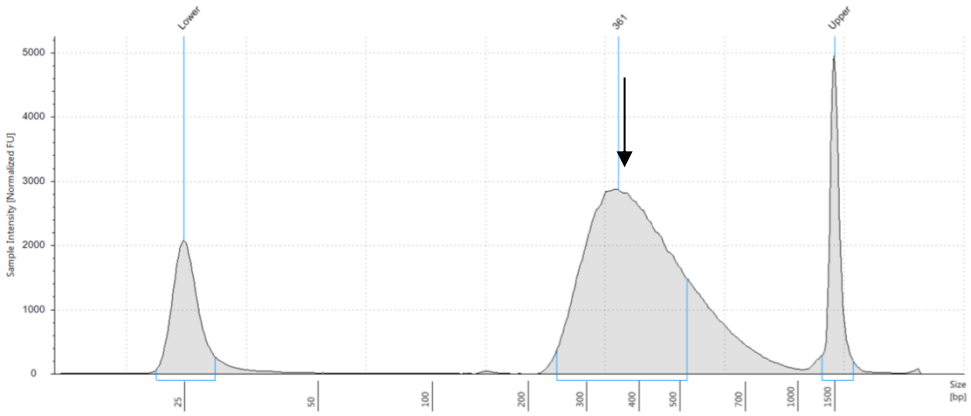

Figure 10 Library check of ganglionic cells of sample GNBn_1

Electropherogram of DNA of the library constructed from ganglionic cells of sample GNBn_1 showing the distribution of fragment sizes. The average size of DNA of ganglionic cells was about 300-400 bp.

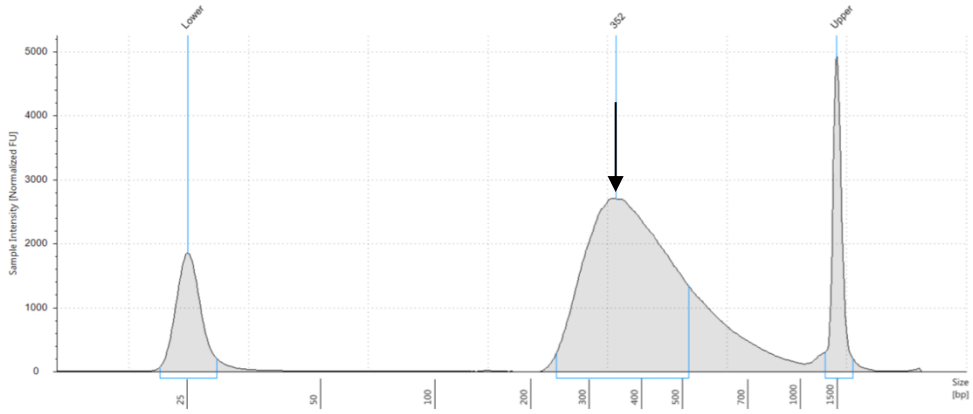

Figure 11 Library check of neuroblasts of sample GNBn_1

Electropherogram of DNA of the library constructed from ganglionic cells of sample GNBn_1 showing the distribution of fragment sizes. The average of size of DNA of neuroblasts was about 300-400 bp.

4.3. Establishing a protocol to create genomic libraries from isolated DNA of single cells

4.3.1. Sample quality, not library preparation determines sequencing quality

To ensure successful whole-genome sequencing, a comparative analysis of different library construction protocols was performed. We decided to sequence the sample first with a cost-effective coverage of 1x instead of 30x. We compared the three different methods of library construction in 3 samples. The samples include microdissected ganglionic cells from case GNBn_2, GNBn_4 and M-GNBi-04.

In method 1, isolated DNA from microdissected tissue was used for library construction. In method 2, isolated DNA from microdissected tissue was first whole-genome amplified prior to library construction. In method 3, library construction was performed by direct usage of microdissected tissue. Method 1 was our method of choice.

Measures of mapped reads, duplicate reads, and the mean coverage rate were taken into consideration to decide on which sample to select for whole-genome sequencing in full 30x coverage.

The rate of mapped reads after exclusion of duplicate reads provides an estimate of how many reads out of all reads in total are matched to the human reference genome.

The duplicate rate gives an estimation of how many duplicates a library contains. These duplicates originate from PCR duplicates that accumulate when constructing the genomic Library. Duplicates are automatically being excluded during the whole-genome sequencing data analysis. Exclusion of duplicates leads to a reduced number of reads left for potential matching to the human reference genome. A reduced number of reads can also occur when the material, due to contamination, is not of human origin but derived from different species.

The mean coverage rate gives an estimation of whether reads are being mapped evenly over the genome, or whether certain regions are being over- or underrepresented.

The mapped read rate was similar in method 2 and 3, and slightly lower in method 1 (**Figure 12**). By contrast, the rate of duplicates was largely comparable between the methods, but was mostly influenced by the sample (**Figure 12**). The mean coverage was highest in method 1, but was also affected by the sample (**Figure 13**).

Together, our comparison of the different methods suggests that a main factor for sequencing data quality may be the specimen, and – to a lesser extent – the method of library construction. Limiting the amount of thawing and ensuring the microdissection of correct cells of choice were the factors that helped to maintain the quality of the specimen.

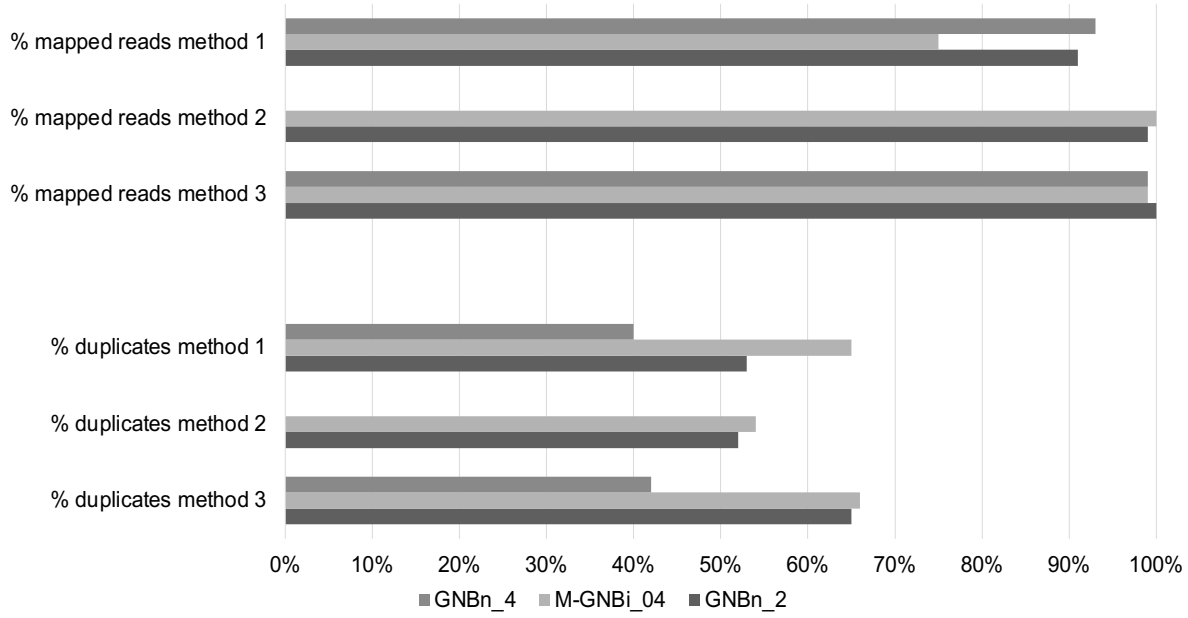

Figure 12 Comparison of mapped read and duplicate rate in sequencing data generated by different library construction protocols

Percentage of mapped reads (top) and read duplicates obtained from sequencing libraries generated by distinct methods. Three different tumor samples were used for library construction (two samples for method 2).

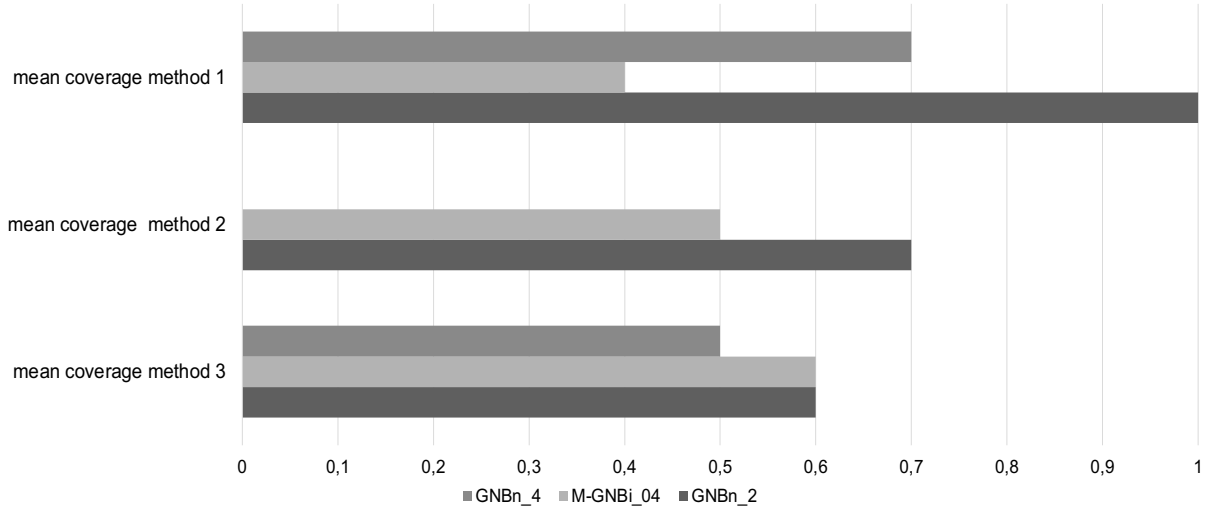

Figure 13 Comparison of mean coverage rate in sequencing data generated by different library construction protocols

Mean coverage rates obtained from sequencing libraries generated by distinct methods. Three different tumor samples were used for library construction (two samples for method 2). Note that mean coverage was highest for case GNBn_2 in each library construction method, and highest in total in method 1 (DNA isolation).

4.4. Neuroblasts and ganglionic cells are clonally related

4.4.1. Higher sequencing coverage in neuroblasts than in ganglionic cells

The sequencing coverage was generally higher in neuroblasts than in ganglionic cells (**Table 14**). The coverage of neuroblasts and ganglionic cells were both high in case GNBn_1, which is why we chose this case to validate mutations exemplarily.

Table 14 Mean coverage of samples

Case	GNBn_1	GNBn_2	GNBn_3	GNBn_4	GNBn_5
NB Coverage	25x	23.8x	11x	29x	16.2x
GC Coverage	22x	2x	0.4x	2.8x	0.3

4.4.2. Shared mutations in neuroblasts and ganglionic cells

Comparison of somatic mutations called in neuroblasts and ganglionic cells of case GNBn_1 revealed that most mutations were detected in both subsets (**Table 15**), which suggests that both cell types may derive from the same clone.

Table 15 Somatic mutations detected case GNBn_1

Abbreviations: x = mutated.

Gene	Chr	Pos	Wildtype	Mutation	Change cDNA	Change Protein	NB	GZ	Validated
MAP2K7	19	7977062	A	T	c.1108A>T	p.K370	X		X
TOX2	20	42683077	A	T	c.790A>T	p.I264F	X		X
GPR6	6	110300739	C	G	c.424C>G	p.L142V	X		X
RRM1	11	4130872	A	T	c.388_splice	e5-2	X		
C2orf53	2	27360790	G	T	c.408C>A	p.S136S	X		
OPA1	3	193376674	A	T	c.2332_splice	e24-2		X	
OPA1	3	193343878	C	A	c.679_splice	e7-3	X	X	
OPA1	3	193355857	A	G	c.1149_splice	e11+3	X	X	
OPA1	3	193364853	G	A	c.1755_splice	e19-1	X	X	
OPA1	3	193374866	T	G	c.2179_splice	e23-3	X	X	
OPA1	3	193361417	G	A	c.1477_splice	e15+1	X	X	
C9orf174	9	100092969	-	GAGGAG	c.2325_2326insGAGGAG	p.E775_E776insEE	X	X	
C11orf16	11	8947499	A	C	c.715T>G	p.W239G	X	X	
C20orf96	20	271226	-	TTA	c.17_splice	e2+2	X	X	
PABPC3	13	25672056	G	A	c.1720G>A	p.G574R	X	X	
PABPC3	13	25672058	G	T	c.1722G>T	p.G574G	X	X	
PABPC3	13	25672073	G	A	c.1737G>A	p.M579I	X	X	
PABPC3	13	25672098	C	G	c.1762C>G	p.L588V	X	X	
PABPC3	13	25672104	T	C	c.1768T>C	p.Y590H	X	X	
PABPC3	13	25672111	T	C	c.1775T>C	p.L592P	X	X	
PABPC3	13	25672126	C	T	c.1790C>T	p.S597L	X	X	
CWF19L2	11	107207442	A	-	c.2203_splice	E16-3	X	X	
PRKD1	14	30396623	-	CCCGGA	c.96_97insTCCGGG	p.P33delinsSGP	X	X	
HIPK2	7	139257974	T	G	c.3296A>C	p.Q1099P	X	X	
CEL	9	135946920	GC	CG	c.2040_2041delinsCG	p.P681A	X	X	
NOL4	18	31523145	A	-	c.1429_splice	e10-3	X	X	

However, several mutations were private to either neuroblasts or ganglionic cells. The presence and absence of two of these mutations, i.e., point mutations in the *TOX2* and *GPR6* gene, were successfully validated in neuroblasts and ganglionic cells, respectively, through dideoxy-sequencing (**Figure 14**).

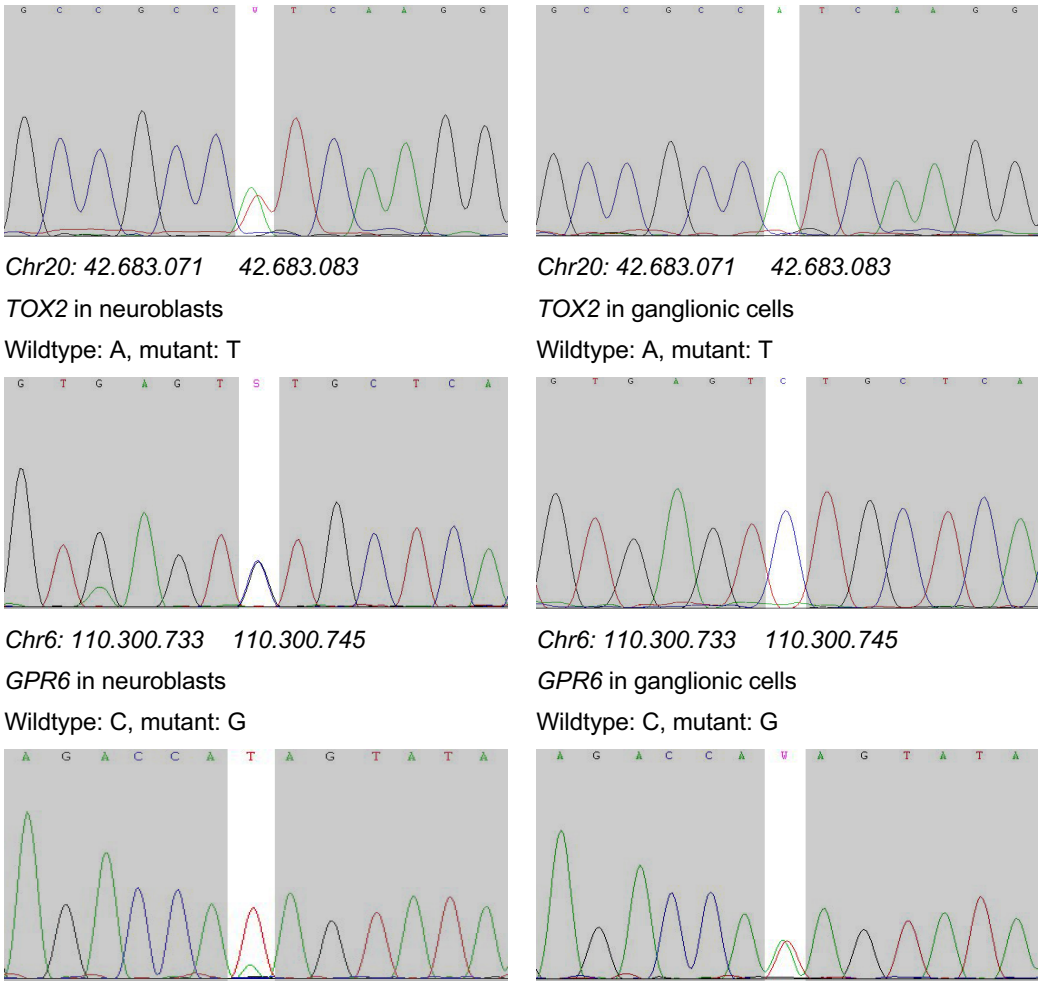

Figure 14 Validation of somatic mutations in tumor cell subtypes by dideoxy-sequencing in case GNBn_1

Sequencing chromatograms of *TOX2*, *GPR6* and *MAP2K7* in neuroblasts and ganglionic cells of case GNBn_1.

TOX2 is thought to play an role in the immune system as it is mainly expressed in the thymus and in immune cells such as CD4 T cells [29], while *GPR6* is an important contributor to neurite growth [30].

Mutations in the genes *C9orf174*, *OPA1* and *PRKD1*, that were called in the WGS data, were not validated by dideoxy-sequencing. According to the WGS mutation calling, mutations in both *C9orf174* and PRKD1 were in-frame insertions. In our in-house pipeline, we have observed that in-frame insertions were disproportionately frequent false positive calls (unpublished). The *OPA1* gene was a highly repetitively called gene within the sequencing

data obtained in this study. Given the overall low mutation frequency in neuroblastoma, such highly mutated genes are also suspects of false-positive calling.

Nevertheless, validation of individual mutations by dideoxy-sequencing supported the reliability of mutation calling in our approach. Also, it provides proof for our hypothesis that neuroblasts and ganglionic cells may be clonally related, but that there are genetic alterations that are private to either of the cell types.

4.5. Identification of biallelic MAP2K7 inactivation in neuroblasts

A homozygous or hemizygous nonsense mutation in the *MAP2K7* gene was identified in neuroblasts of case GNBn_1 **(Table 16).** In addition, a single mutated read was detected in sequencing data of the ganglionic cells, supporting the hypothesis that ganglionic cells and neuroblasts are clonally related. Validation by dideoxy-sequencing revealed a heterozygous mutation in the ganglionic cells, and a homozygous or hemizygous mutation of *MAP2K7* in neuroblasts **(Figure 14).**

Mitogen Activated Protein Kinase Kinase 7, encoded by *MAP2K7* which is located on chromosome 19 in humans, is a critical kinase for activation of the JNK signaling pathway. *MAP2K7* is a family member of an intracellular complex and is activated by extracellular stimuli. Once activated, *MAP2K7* in turn directly activates JNK through phosphorylation, which leads to induction of transcription factors resulting in apoptosis, cell cycle arrest and degeneration of the cell.

The finding of a homozygous or hemizygous mutation in *MAP2K7* in neuroblasts, which occurred as heterozygous mutation in ganglionic cells, indicated that biallelic inactivation may contribute to the malignant phenotype of neuroblasts. More specifically, this result suggest that biallelic inactivation of the *MAP2K7* gene and consecutively impaired JNK signaling may promote tumorigenesis in neuroblastic tumors by inhibiting neural differentiation and impairing apoptosis.

To determine whether *MAP2K7* is recurrently mutated in neuroblastic tumors, we screened our sequencing database and found five additional cases that harbored *MAP2K7* mutations. Intriguingly, all tumors had evidence of biallelic *MAP2K7* inactivation, conferred by single nucleotide variants on the one allele, and deletion of the other allele (**Figure 15**). Single nucleotide variants led to premature stop codons in 2 cases, and to missense and splice site mutations in 2 and 1 cases, respectively. All mutations occured in the kinase domain region of

MAP2K7. Regions affected by copy number loss varied between samples, but covered the *MAP2K7* locus in all cases.

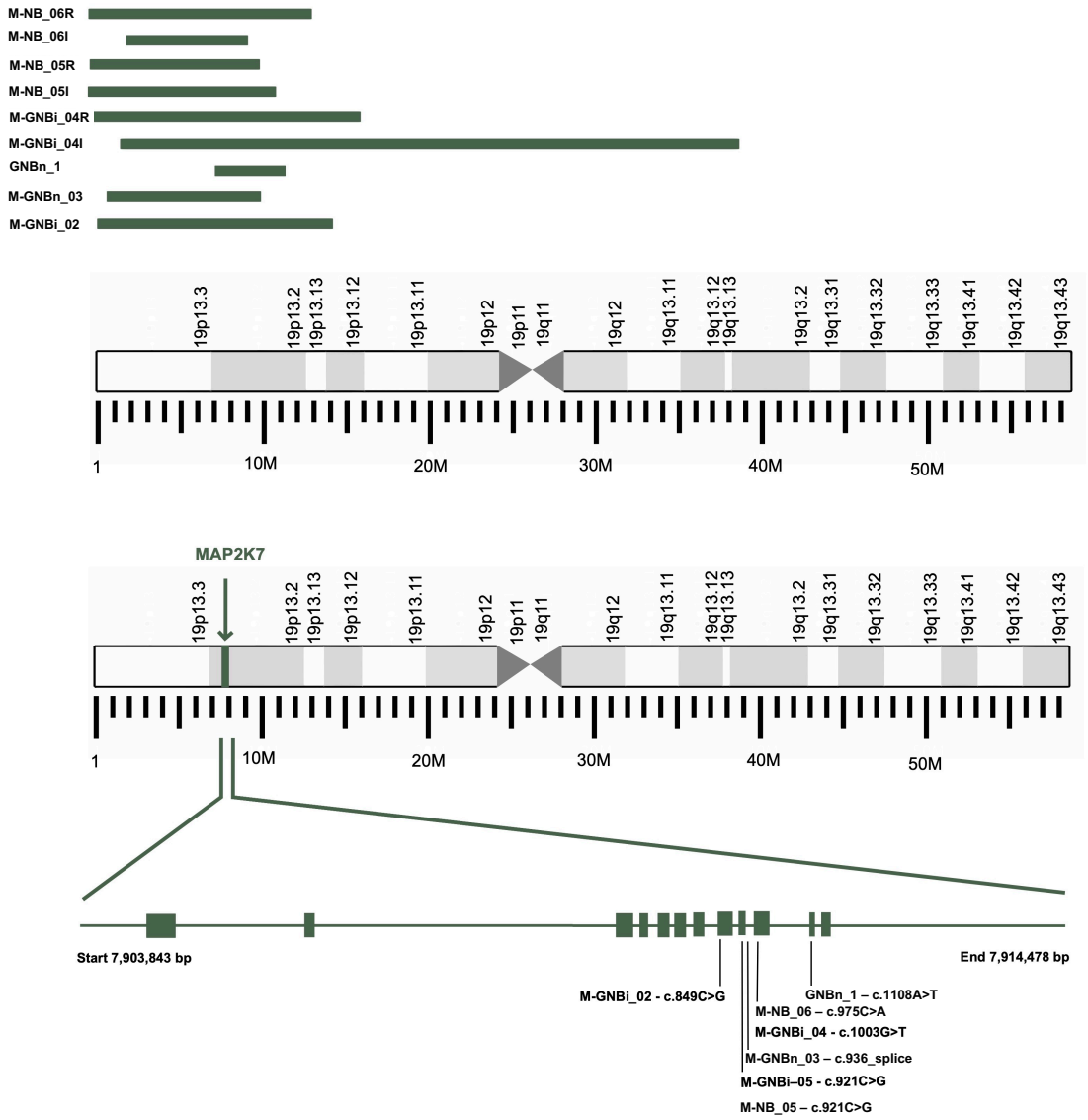

Figure 15 Biallelic inactivation of *MAP2K7* in neuroblastic tumors

Green bars on top of schematic chromosomes show the regions of deletion on chromosome19 within each case, including initial (I) and relapse (R) tumors. The *MAP2K7* locus was always located within the deleted region. Green bars below schematic chromosomes show the different point mutations identified within the *MAP2K7* gene in each case.

All single nucleotide variants were validated by dideoxy-sequencing (**Figure 16**). Deletions of chromosome 19p regions were validated by FISH analysis (data not shown).

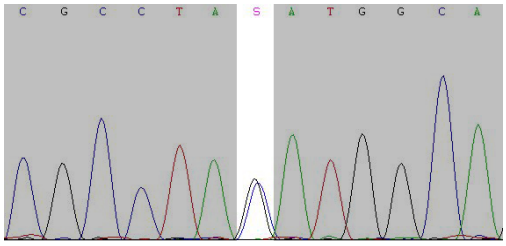

Chr19:7.976.032 *Chr19:7.976.044*
Case M-GNBi_02: Bulk
Wildtype: C, mutant: G

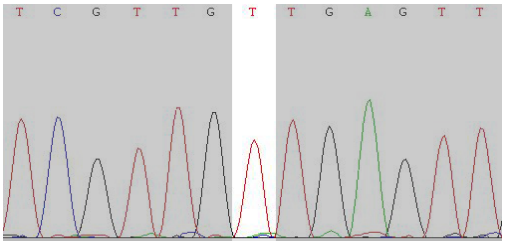

Chr19:7.976.210 *Chr19:7.976.222*
Case M-GNBn_03: Bulk
Wildtype: G, mutant: T

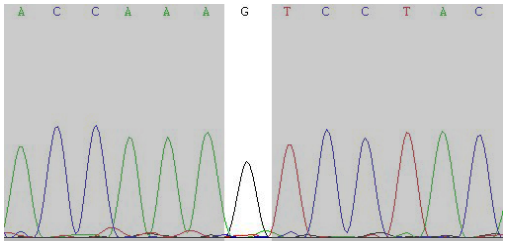

Chr19:7.976.381 *Chr19:7.976.393*
Case M-GNBi_04 initial: Bulk
Wildtype: G, mutant: T

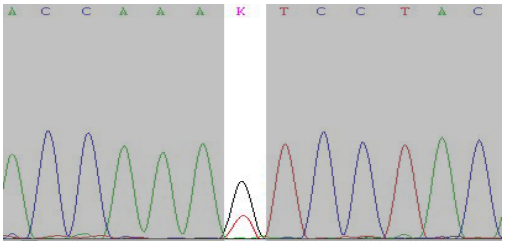

Chr19:7.976.381 *Chr19:7.976.393*
Case M-GNBi_04 relapse: Bulk
Wildtype: G, mutant: T

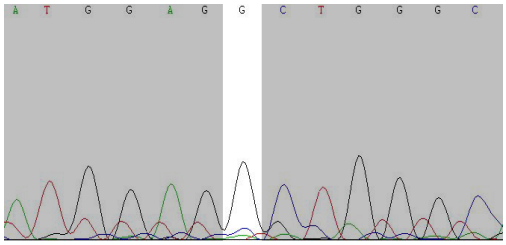

Chr19: 7.976.194 *Chr19:7.976.206*
Case M-NB_05 initial: Bulk
Wildtype: C, mutant: G

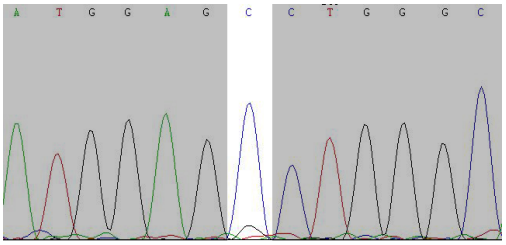

Chr19: 7.976.194 *Chr19:7.976.206*
Case M-NB_05 relapse: Bulk
Wildtype: C, mutant: G

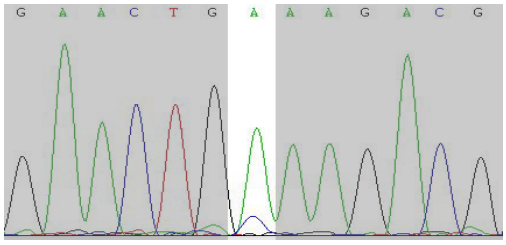

Chr19:7.976.353 *Chr19:7.976.365*
Case M-NB_06 initial
Wildtype: C, mutant: A

Figure 16 Validation of *MAP2K7* mutations through dideoxy-sequencing
Sequencing chromatograms of *MAP2K7* in neuroblastic tumors.

All children whose tumors harbored *MAP2K7* mutations were considered high-risk patients. All of them were older than 18 months at diagnosis, and had stage 4 disease (**Table 16**). In addition, progression or relapse occurred in all patients, except for one case in which follow-up was missing. By contrast, comprehensive analysis of genomic alterations occurring in *MAP2K7* mutated neuroblastic tumors revealed that these cases did not show any mutations associated with telomere maintenance mechanisms which are found frequently in high-risk neuroblastoma: The tumors neither harbored *ATRX* mutations, nor *MYCN* amplification or *TERT* rearrangements (**Table 17**).Together, these findings suggest that tumors with biallelic inactivation of *MAP2K7* may represent a new subtype of high-risk neuroblastoma.

Table 16 Clinical features of patients whose tumors harbored MAP2K7

Abbreviations: GNBn = ganglioneuroblastoma, nodular subtype, GNBi = ganglioneuroblastoma, intermixed, NBg/diff = neuroblastoma poorly differentiated, d = days. Dx = diagnosis EFS = event-free survival. OS = overall survival.

Case	Histology	Stage	Age in d at Dx	Event	EFS	Survival	OS
GNBn_1	GNBn	4	3672	Relapse	2105	No	2828
M-GNBi_02	GNB (not specified)	4	681	Not specified	Not specified	Not specified	Not specified
M-GNBn_03	GNBn	4	4785	Progress	414	No	1327
M-GNBi_04	GNBi	4	1109	Progress	574	Yes	1578
M-NB_05	NBg/diff	4	2268	Progress	165	No	249
M-NB_06	NBg/diff	4	2022	Progress	1091	No	1578

Table 17 Genetic features of MAP2K7 cases related to telomere maintenance

Case	ATRX	TERT rearrangement	MYCN amplification
GNBn_1	/	/	/
M-GNBi_02	/	/	/
M-GNBn_03	/	/	/
M-GNBi_04	/	/	/
M-NB_05	/	/	/
M-NB_06	/	/	/

4.6. Identification of an *ATRX* mutation in neuroblasts in case GNBn_4

Analysis of WGS data of case GNBn_4 revealed an *ATRX* splice site mutation in the neuroblast population, which was validated through dideoxy-sequencing (**Figure 17**). The coverage of 2.8x obtained in sequencing data of ganglionic cells was too low to analyze the genomic status of *ATRX*. However, dideoxy-sequencing of ganglionic cells of this case revealed no mutation of *ATRX* at the position mutated in neuroblasts.

As mutations of *ATRX* are associated with activation of the Alternative Lengthening of Telomeres (ALT) pathway [31], this finding points towards ALT in the neuroblastic component of this tumor.

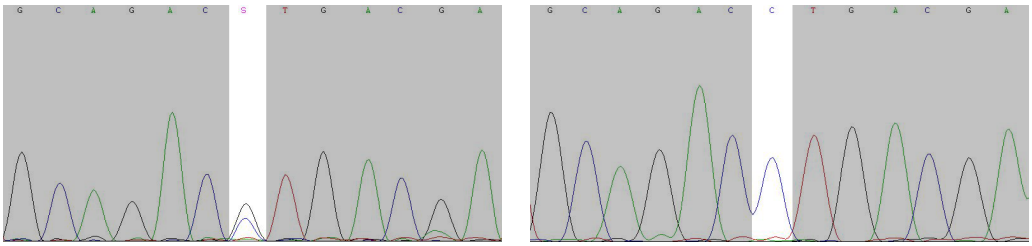

ChrX: 76.909.685 *ChrX: 76.909.697*
Case GNBn_4: neuroblasts
Gene: ATRX
Wildtype: C, **mutant:** G

ChrX: 76.909.685 *ChrX: 76.909.697*
Case GNBn_4: ganglionic cells
Gene: ATRX
Wildtype: C**, mutant:** G

Figure 17 Validation of an *ATRX* mutation through dideoxy-sequencing
Sequencing chromatograms of *ATRX* in neuroblasts and ganglionic cells of GNBn_4.

4.7. Ganglionic cells in GNBn are senescent

4.7.1. Optimization of β-galactosidase staining for senescence detection

Senescence is the state in which cells irreversibly enter into cell-cycle arrest and no longer divide. The enzyme ß-galactosidase accumulates in senescent cells. The addition of x-gal leads to its hydrolyzation by ß-gal into a blue chromogen. Thus, these dormant cells can be detected by positive staining for senescence-associated ß-galactosidase. [32]

Different pH levels have been tested to optimize the staining protocol (**Table 18**). The lower the pH level was, the more intense was the blue signal. However, we also observed that the lower the pH level was, the higher the noise and false positive staining of surrounding tissue was (**Figure 18**), which is why we finally decided to stain with an intermediate pH level of 5.88.

Table 18 pH levels used for ß-galactosidase staining

Fixative Solution	**No addition of HCl**	**pH 6.13**
15 ml Staining Solution	Addition of 40 µl 1 N HCl	pH 5.95
15 ml Staining Solution	Addition of 80 µl 1 N HCl	pH 5.88
15 ml Staining Solution	Addition of 120 1 N HCl	pH 5.7

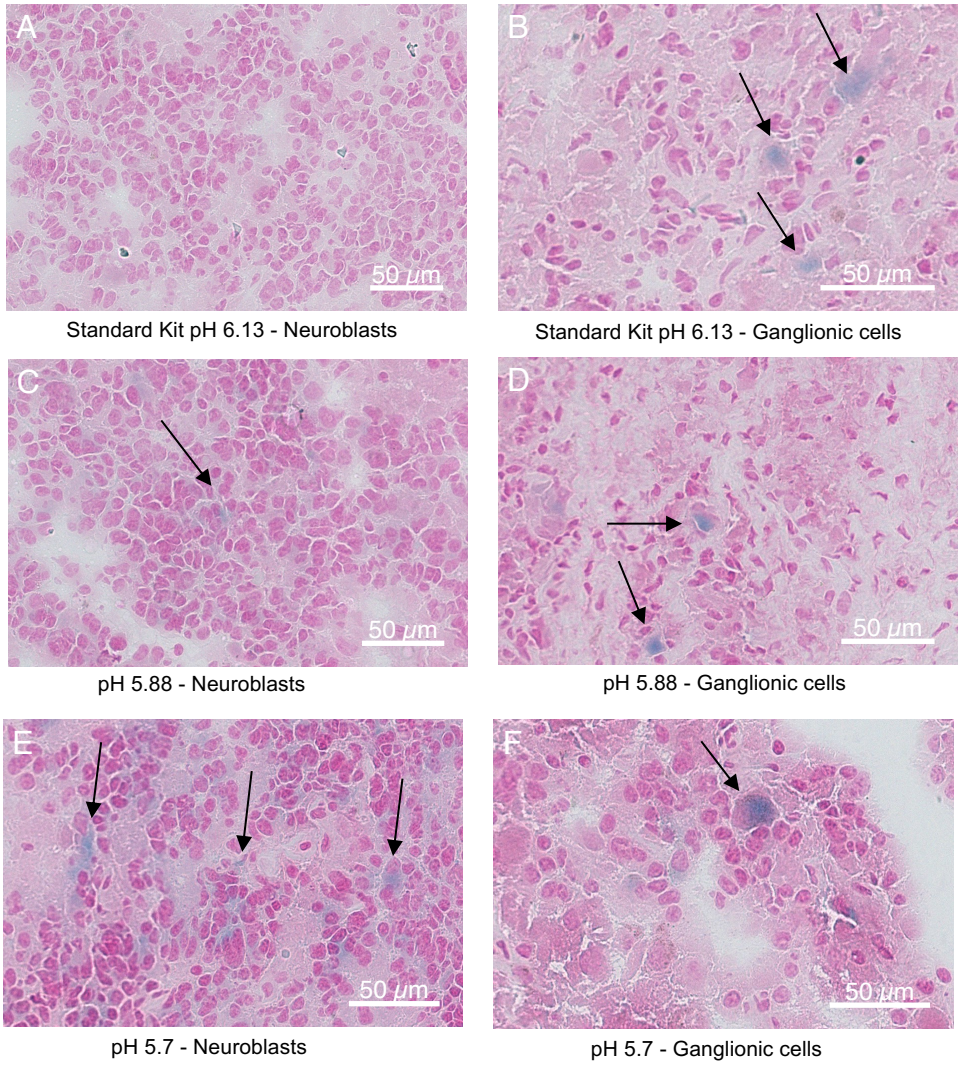

Figure 18 Testing of various pH values for β-galactosidase staining

(**A**) Negative staining of neuroblasts at pH 6.1. (**B**) Positive staining of ganglionic cells at pH 6.1. (**C**) Negative staining of neuroblasts with hints of signal noise at pH 5.8. (**D**) Positive staining of ganglionic cells at pH 5.8. (**E**) Negative staining of neuroblasts with obvious signal noise at pH 5.7. (**F**) Positive staining of an individual ganglionic cells with signal noise in other cells at pH 5.7.

Senescence staining was successfully performed on five GNBn cases selected for this study (**Figure 19**) The staining results of case GNBn_3 were not evaluable (data not shown). Neuroblasts were senescent-negative in all cases, while ganglionic cells were generally senescent-positive, although some variability was observed. We assume that the variation of senescence-positivity in ganglionic cells may be due to possible degradation of the enzyme in samples that have been stored for many years (**Table 19**).

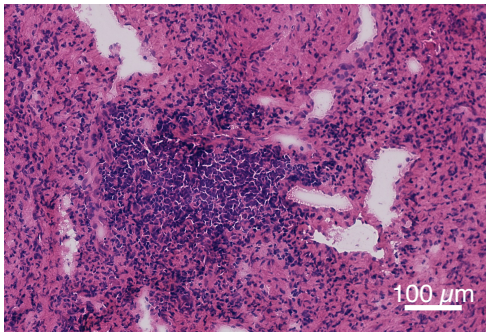

GNBn_1: H&E staining of neuroblasts

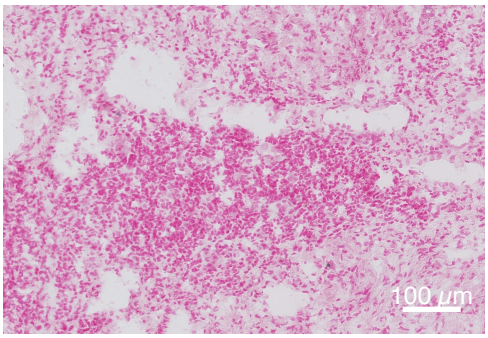

GNBn_1: ß-galactosidase staining of neuroblasts

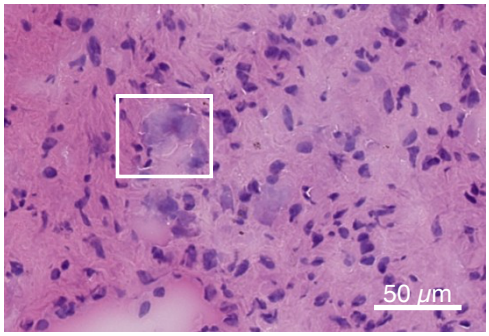

GNBn_1: H&E staining of ganglionic cells

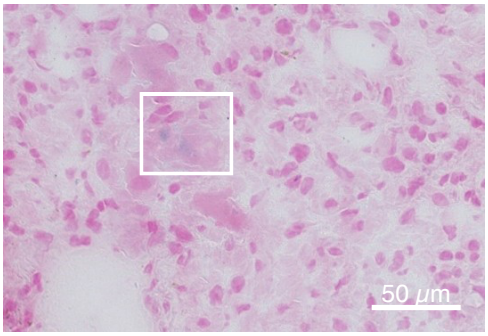

GNBn_1: ß-galactosidase staining of ganglionic cells

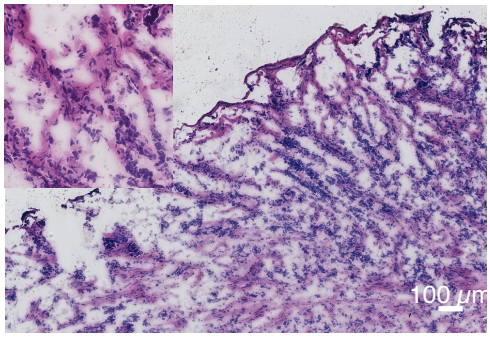

GNBn_2: H&E staining of neuroblasts

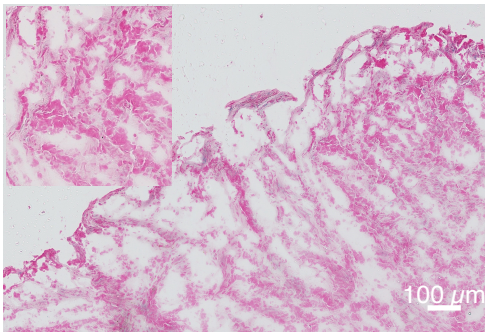

GNBn_2: ß-galactosidase staining of neuroblasts

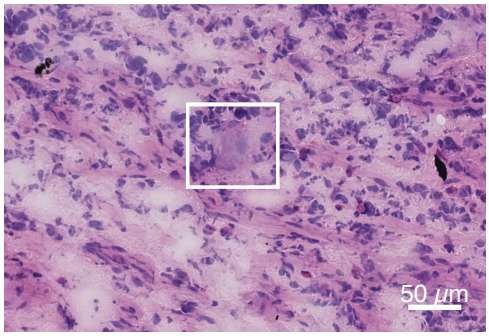

GNBn_2: H&E staining of ganglionic cells

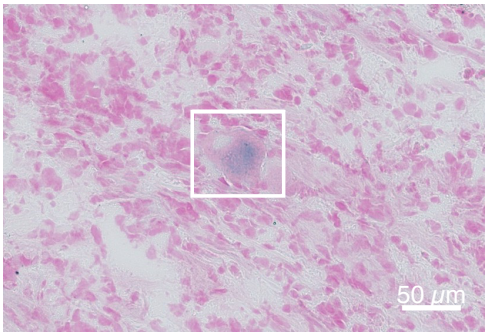

GNBn_2: ß-galactosidase staining of ganglionic cells

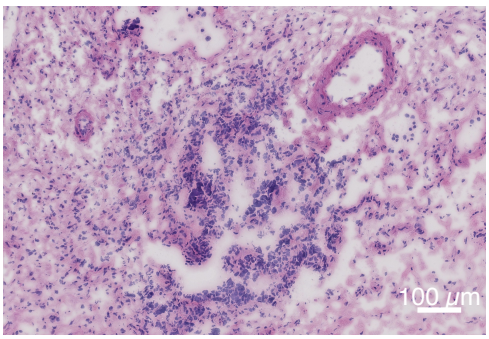

GNBn_4: H&E staining of neuroblasts

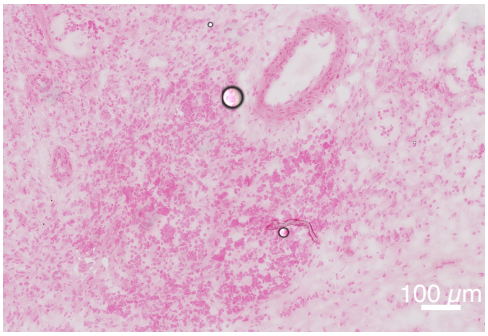

GNBn_4: ß-galactosidase staining of neuroblasts

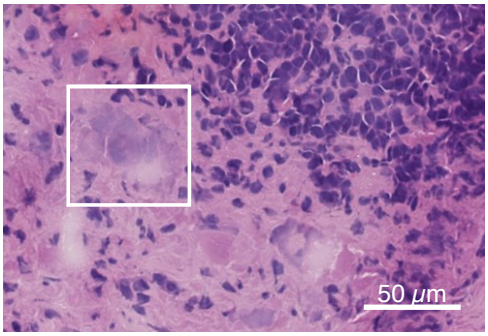

GNBn_4: H&E staining of ganglionic cells

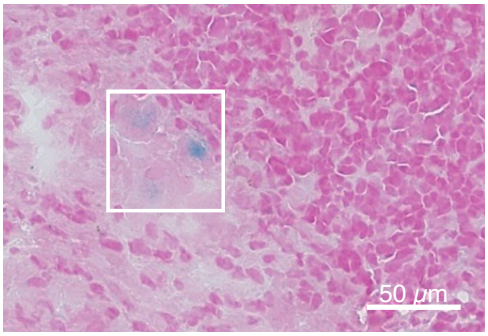

GNBn_4: ß-galactosidase staining of ganglionic cells

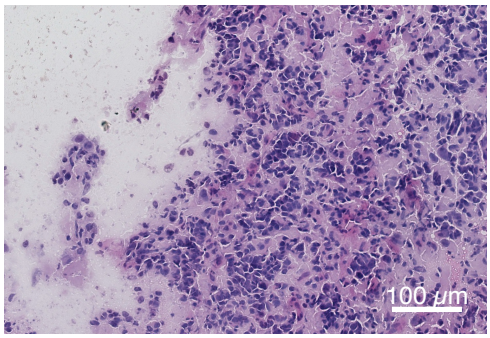

GNBn_5: H&E staining of neuroblasts

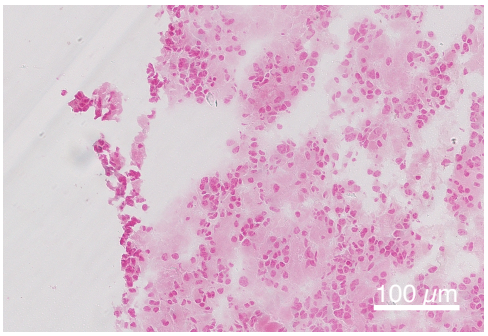

GNBn_5: ß-galactosidase staining of neuroblasts

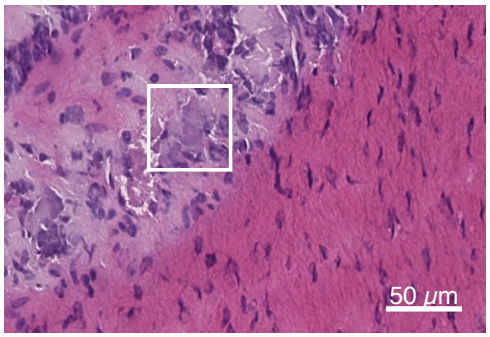

GNBn_5: H&E staining of ganglionic cells

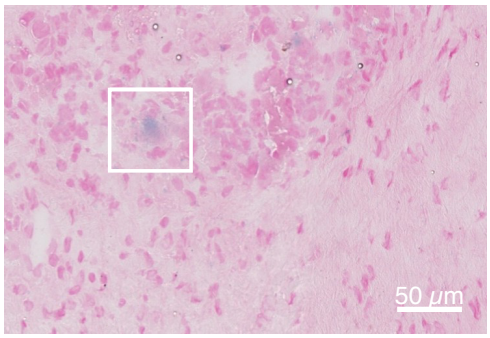

GNBn_5: ß-galactosidase staining of ganglionic cells

Figure 19 Results of β-galactosidase staining of ganglioneuroblastoma cases

Neuroblasts consistently stained negative for β-galactosidase, whereas ganglionic cells consistently stained positive (blue), indicating senescence of these cells.

Table 19 Features of specimens examined by ß-galactosidase staining

Case	Neuroblasts	Ganglionic Cells	Collection date of specimen
GNBn_1	Negative	Positive	1997
GNBn_2	Negative	Positive	2000
GNBn_3	Not evaluable	Not evaluable	2011
GNBn_4	Negative	Positive	2011
GNBn_5	Negative	Positive	2016

5. Discussion

The aim of this study was to determine the mutation profile and clonal relationship of ganglionic and neuroblastic cells occurring in GNBn. The study demonstrated that ganglionic and neuroblastic cells are clonally related, as they shared several mutations. We also found evidence, however, that neuroblasts harbor private genomic alterations, such as inactivating mutations of *MAP2K7* and *ATRX*, which may account for the malignant properties of this cell type and their inability to differentiate. By contrast, malignant neuroblasts may differentiate into senescent ganglionic cells in the absence of such mutations.

In this study, LCM was used to dissect individual cells or cell clusters from GNBn for massive parallel sequencing analysis. LCM is a well-established approach for genomic analyses of single cells identified in tissue sections. This technique allows for specific analysis of morphologically or immunohistochemically defined cell populations. A potential limitation of this technique, however, is its susceptibility to contamination of cells located in proximity to the target cells. Selection of cells can also be difficult, as the quality of histological appearance is affected by the lack of cover slipping the slides. Immunohistochemical staining may help to improve the specificity and precision of identifying target cells. However, immunohistochemical staining may also add to degradation of DNA, leading to suboptimal sequencing results [28]. DNA integrity may also be affected by experimental steps preceding DNA analysis, such as fixation of the tissue or thawing of the tissue. In this study, only fresh-frozen samples have been analyzed, as fixation with formalin accelerates DNA degradation. Nevertheless, excessive fragmentation of DNA was observed in some tumor samples analyzed in this study. HE staining of the tumor sections prior to LCM is known to alter RNA integrity [28,33], which may also apply to DNA.

Another potential limitation of this study may arise from the broad spectrum of histological appearance of neuroblastic tumors with fluent transitions, which may impede assignment of the tumor to one of four histological INPC categories in some instances. The identity and differentiation state of individual cells may not always be unequivocal, as large neuroblasts in poorly differentiated neuroblastoma resemble ganglionic cells [13]. Similarly, ganglionic cells in neuroblastic tumors are heterogenous in morphology and state of differentiation. It is conceivable that cells in earlier stages of differentiation may harbor different genetic alterations than cells in advanced stages. As the differentiation pathway from neuroblasts to ganglionic cell is thought to be continuous [1,2], it may be difficult to monitor changes in genomic profiles at the various differentiation stages, at least with the low- to medium-throughput approach that was used in this study. We therefore decided to examine cell types corresponding to the extremes of the differentiation spectrum, i.e., undifferentiated or poorly differentiated

neuroblasts and terminally differentiated ganglionic cells. Still, genetic similarities observed between neuroblasts and ganglionic cells could have been caused by cross-contamination of either cell type, including the heterozygous *MAP2K7* mutation detected in ganglionic cells.

Despite these potential limitations, we were able to obtain meaningful mutational profiles of neuroblastic and ganglionic cells in several cases of GNBn and to determine shared and private alterations in these two cell types, similar to studies in other cancer types [34]. Novel single cell sequencing approaches with higher throughput, which have been developed over recent years [35], may further improve the sensitivity and accuracy of detecting genomic alterations in the entire spectrum of malignant cells occurring in GNBn.

The results of this study suggest that neuroblasts and ganglionic cells in GNBn may have the same clonal origin, as suggested by others previously [14]. It thus remains a key question, which molecular alterations promote or inhibit neuronal differentiation in ganglionic cells and neuroblasts, respectively. Apart from the differentiated morphology, we also noted in this study that ganglionic cells, as opposed to neuroblasts, stained positive for beta-galactosidase, indicating senescence of these cells. Three types of DNA damaging stimuli can elicit senescence: First, DNA damage (DNA damage-induced senescence), e.g., through treatment with cytotoxic agents in cancer therapy, can trigger cells to escape into senescence. Second, loss of a tumor suppressor gene (oncogene-induced senescence) can drive cells into senescence to prevent malignant transformation of the cell [32]. Third, telomere shortening (replicative senescence) can lead to senescence. Telomere shortening is the result of repeated DNA replication, as the ends of linear chromosomes cannot be fully elongated by the replication machinery. Once a critical length of the telomeres is reached, cells stop to divide and may undergo senescence (Hayflick limit). [32,36].

As we found evidence in our study that genetic alterations associated with telomere maintenance, i.e., *ATRX* and potentially also *MAP2K7* mutations, occur exclusively in malignant neuroblasts, but not in ganglionic cells of GNBn, we hypothesize that shortening of telomeres and consecutive replicative senescence is responsible for senescence of the latter. Theoretically, senescence staining may also be positive in neuroblasts after DNA damage due to chemotherapy, or loss of a tumor suppressor gene. However, we did not observe senescence in neuroblasts in the pretreatment samples that had been analyzed in this study. Our data thus suggest that malignant neuroblasts in GNBn differ from ganglionic cells by activation of telomere maintenance mechanisms, allowing them to escape from senescence and to proliferate infinitely. The finding of an *ATRX* mutation in one case suggest that not telomerase but the alternative lengthening of telomeres (ALT) pathway had been activated in

neuroblasts of this tumor. Activation of ALT can be evaluated by detection of ALT-associated PML nuclear bodies, which would allow to assess ALT in neuroblasts and ganglionic cells on the single cell level [9,37]. Thus, further analyses are needed to test our hypothesis that the telomere maintenance status is a discriminating factor between malignant neuroblasts and ganglionic cells in GNBn.

While basic principles of the molecular pathogenesis of neuroblastoma have been elucidated in recent years, many questions have remained unresolved. The vast majority of high-risk cases harbor genomic alterations of *MYCN*, *TERT*, or *ATRX*, all converging on activation of telomere maintenance [12]. In this study, we found biallelicly inactivating mutations of *MAP2K7* in high-risk tumors that lack all the alterations mentioned above, which has not been described in neuroblastoma before. This finding suggests that biallelic mutation of *MAP2K7* may be a driving event in a subgroup of high-risk neuroblastoma.

The mitogen activated protein kinase kinase 7, which is encoded by *MAP2K7*, specifically phosphorylates JNK. Various intracellular processes are regulated by JNK such as cell cycle arrest, cellular differentiation, apoptosis and tumor metabolism [38]. Studies show that a loss of *MAP2K7* and JNK activity can promote tumorigenesis by disrupting cell cycle arrest [39]. It therefore can be concluded that the *MAP2K7*-JNK-pathway is crucial to cellular homeostasis and may act as protective barrier against malignant transformation.

Although different isoforms of MAP kinases are involved in phosphorylation of JNK, mono-phosphorylation by *MAP2K7* alone is sufficient for JNK activity [40,41]. In addition, the JNK pathway is severely impaired if *MAP2K7* inactivated. Analysis in various cancer types suggest that a compromised *MAP2K7* and JNK signaling pathway promotes tumorigenesis [42-44]. In neuroblastoma, it has been suggested that the JNK pathway may be crucial for neuronal differentiation [45,46]. Furthermore, a decreased activity of JNK has been observed in neuroblastoma cell lines [47]. Taking these findings together, it is tempting to speculate that biallelic inactivation of *MAP2K7* may promote neuroblastoma tumorigenesis by inhibiting neuronal differentiation and cell cycle arrest. In addition, it is likely that malignant cells of these tumors have acquired telomere maintenance mechanisms, since continuous proliferation in the absence of TMM would inevitably lead to telomere attrition and consecutively programmed cell death. We therefore propose a model on the role of *MAP2K7* in neuroblastoma pathogenesis (**Figure 20**).

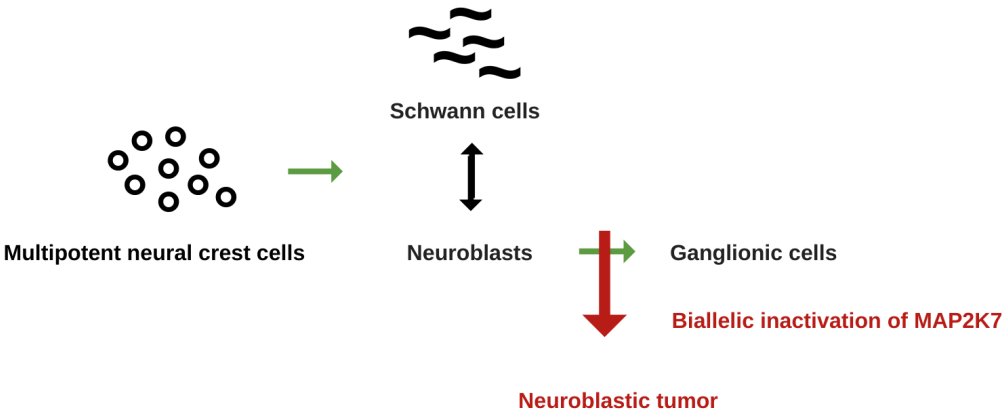

Figure 20 Model of malignant transformation in neuroblastic tumors harboring inactivating mutations of *MAP2K7.*

Multipotent neural crest cells develop into Schwann cells and neuroblasts. Neuroblasts in turn are supposed to differentiate into ganglionic cells. Neuroblasts and Schwann cells interact with each other. *MAP2K7* is a protein that is vital for neural differentiation. If a biallelic mutation in the *MAP2K7* gene occurs, differentiation is inhibited and neuroblasts may transform into malignant cells.

As a future perspective, modulating *MAP2K7* activity in experimental model systems would be required to validate the gene's mechanistic relevance for neuroblastic tumor development and progression. A *MAP2K7* knockdown approach in mice demonstrated potential neural degeneration[48]. Another study found that inactivation of *MAP2K7* accelerates tumorigenesis [39]. In addition, a knockdown or knockout of *MAP2K7* in cell lines may provide further evidence for the role of *MAP2K7* in neuroblastoma pathogenesis. Furthermore, the exact frequency of *MAP2K7* mutations and their association with clinical covariates need to be determined in larger cohorts, using either genomic data or immunohistochemistry to detect loss of MAP2K7 expression on the protein level. It would also be interesting to see whether JNK signaling is inactivated by other alterations in additional cases of neuroblastoma.

In conclusion, the finding of biallelic inactivation of *MAP2K7* provides new insights into the pathophysiology behind neuroblastic tumors. In-depth analysis of the molecular consequences of *MAP2K7* inactivation may create new opportunities for developing targeted therapies to combat this deadly pediatric disease.

6. References

1. Louis CU, Shohet JM. Neuroblastoma: Molecular Pathogenesis and Therapy. *Annual Review of Medicine* 2015; **66**(1): 49-63.
2. Tomolonis JA, Agarwal S, Shohet JM. Neuroblastoma pathogenesis: deregulation of embryonic neural crest development. *Cell and Tissue Research* 2018; **372**(2): 245-62.
3. Bunimovich YL, Keskinov AA, Shurin GV, Shurin MR. Schwann cells: a new player in the tumor microenvironment. *Cancer Immunology, Immunotherapy* 2017; **66**(8): 959-68.
4. Weiss T, Taschner-Mandl S, Bileck A, et al. Schwann cell plasticity regulates neuroblastic tumor cell differentiation. *bioRxiv* 2020: 2020.04.01.019422.
5. Neuroblastoma (Pediatric Oncology): Springer; 2005.
6. Monclair T, Brodeur GM, Ambros PF, et al. The International Neuroblastoma Risk Group (INRG) staging system: an INRG Task Force report. *J Clin Oncol* 2009; **27**(2): 298-303.
7. Brodeur GM. Neuroblastoma: biological insights into a clinical enigma. *Nat Rev Cancer* 2003; **3**(3): 203-16.
8. Hanahan D, Weinberg RA. Hallmarks of cancer: the next generation. *Cell* 2011; **144**(5): 646-74.
9. Gaspar TB, Sá A, Lopes JM, Sobrinho-Simões M, Soares P, Vinagre J. Telomere Maintenance Mechanisms in Cancer. *Genes (Basel)* 2018; **9**(5).
10. Henson JD, Neumann AA, Yeager TR, Reddel RR. Alternative lengthening of telomeres in mammalian cells. *Oncogene* 2002; **21**(4): 598-610.
11. Peifer M, Hertwig F, Roels F, et al. Telomerase activation by genomic rearrangements in high-risk neuroblastoma. *Nature* 2015; **526**(7575): 700-4.
12. Ackermann S, Cartolano M, Hero B, et al. A mechanistic classification of clinical phenotypes in neuroblastoma. *Science (New York, NY)* 2018; **362**(6419): 1165-70.
13. Shimada H, Ambros IM, Dehner LP, Hata J, Joshi VV, Roald B. Terminology and morphologic criteria of neuroblastic tumors: recommendations by the International Neuroblastoma Pathology Committee. *Cancer* 1999; **86**(2): 349-63.
14. Angelini P, Baruchel S, Marrano P, Irwin MS, Thorner PS. The neuroblastoma and ganglion components of nodular ganglioneuroblastoma are genetically similar: evidence against separate clonal origins. *Mod Pathol* 2015; **28**(2): 166-76.
15. Angelini P, London WB, Cohn SL, et al. Characteristics and outcome of patients with ganglioneuroblastoma, nodular subtype: a report from the INRG project. *Eur J Cancer* 2012; **48**(8): 1185-91.
16. Shimada H, Umehara S, Monobe Y, et al. International neuroblastoma pathology classification for prognostic evaluation of patients with peripheral neuroblastic tumors: a report from the Children's Cancer Group. *Cancer* 2001; **92**(9): 2451-61.
17. Teshiba R, Kawano S, Wang LL, et al. Age-Dependent Prognostic Effect by Mitosis-Karyorrhexis Index in Neuroblastoma: A Report from the Children's Oncology Group. *Pediatric and Developmental Pathology* 2014; **17**(6): 441-9.
18. Peuchmaur M, d'Amore ES, Joshi VV, et al. Revision of the International Neuroblastoma Pathology Classification: confirmation of favorable and unfavorable prognostic subsets in ganglioneuroblastoma, nodular. *Cancer* 2003; **98**(10): 2274-81.
19. Umehara S, Nakagawa A, Matthay KK, et al. Histopathology defines prognostic subsets of ganglioneuroblastoma, nodular. *Cancer* 2000; **89**(5): 1150-61.
20. He WG, Yan Y, Tang W, Cai R, Ren G. Clinical and biological features of neuroblastic tumors: A comparison of neuroblastoma and ganglioneuroblastoma. *Oncotarget* 2017; **8**(23): 37730-9.
21. Schmidt ML, Salwen HR, Chagnovich D, Bauer KD, Crawford SE, Cohn SL. Evidence for Molecular Heterogeneity in Human Ganglioneuroblastoma. *Pediatric Pathology* 1993; **13**(6): 787-96.
22. Yamazaki F, Nakazawa A, Osumi T, et al. Two cases of neuroblastoma comprising two distinct clones. *Pediatr Blood Cancer* 2014; **61**(4): 760-2.
23. Shimada H, Ambros IM, Dehner LP, et al. The International Neuroblastoma Pathology Classification (the Shimada system). *Cancer* 1999; **86**(2): 364-72.

24. MicroImaging CZ. Palm Protocols - DNA Handling. 2011. https://www.urmc.rochester.edu/MediaLibraries/URMCMedia/confocal-microscopy-core/documents/ZEISS-DNA-handling.pdf.
25. Datta S, Malhotra L, Dickerson R, Chaffee S, Sen CK, Roy S. Laser capture microdissection: Big data from small samples. *Histol Histopathol* 2015; **30**(11): 1255-69.
26. Nguyet Kong WN, Lucy Cai, Alvin Leonardo, Bart C. Weimer. Integrating the DNA Integrity Number (DIN) to Assess Genomic DNA (gDNA) Quality Control Using the Agilent 2200 TapeStation System. 2014.
27. G P Dimri XL, G Basile, M Acosta, G Scott, C Roskelley, E E Medrano, M Linskens, I Rubelj, O Pereira-Smith. A biomarker that identifies senescent human cells in culture and in aging skin in vivo. *Proc Natl Acad Sci U S A* 1995; **92**(20).
28. Mahalingam M. Laser Capture Microdissection: Insights into Methods and Applications. In: Murray GI, ed. Laser Capture Microdissection: Methods and Protocols. New York, NY: Springer New York; 2018: 1-17.
29. Yu X, Li Z. TOX gene: a novel target for human cancer gene therapy. *Am J Cancer Res* 2015; **5**(12): 3516-24.
30. Tanaka S, Ishii K, Kasai K, Yoon SO, Saeki Y. Neural expression of G protein-coupled receptors GPR3, GPR6, and GPR12 up-regulates cyclic AMP levels and promotes neurite outgrowth. *J Biol Chem* 2007; **282**(14): 10506-15.
31. Heaphy CM, de Wilde RF, Jiao Y, et al. Altered telomeres in tumors with ATRX and DAXX mutations. *Science (New York, NY)* 2011; **333**(6041): 425.
32. Zeng S, Shen W, Liu L. Senescence and Cancer. *Cancer Translational Medicine* 2018; **4**(3): 70-4.
33. Wang H, Owens JD, Shih JH, Li MC, Bonner RF, Mushinski JF. Histological staining methods preparatory to laser capture microdissection significantly affect the integrity of the cellular RNA. *BMC Genomics* 2006; **7**: 97.
34. Fend F, Quintanilla-Martinez L, Kumar S, et al. Composite low grade B-cell lymphomas with two immunophenotypically distinct cell populations are true biclonal lymphomas. A molecular analysis using laser capture microdissection. *Am J Pathol* 1999; **154**(6): 1857-66.
35. Jia Q, Chu H, Jin Z, Long H, Zhu B. High-throughput single-cell sequencing in cancer research. *Signal Transduction and Targeted Therapy* 2022; **7**(1): 145.
36. Gorgoulis V, Adams PD, Alimonti A, et al. Cellular Senescence: Defining a Path Forward. *Cell* 2019; **179**(4): 813-27.
37. Chung I, Osterwald S, Deeg KI, Rippe K. PML body meets telomere: the beginning of an ALTernate ending? *Nucleus* 2012; **3**(3): 263-75.
38. Park JG, Aziz N, Cho JY. MKK7, the essential regulator of JNK signaling involved in cancer cell survival: a newly emerging anticancer therapeutic target. *Therapeutic Advances in Medical Oncology* 2019; **11**: 1758835919875574.
39. Schramek D, Kotsinas A, Meixner A, et al. The stress kinase MKK7 couples oncogenic stress to p53 stability and tumor suppression. *Nature genetics* 2011; **43**(3): 212-9.
40. Finch A, Holland P, Cooper J, Saklatvala J, Kracht M. Selective activation of JNK/SAPK by interleukin-1 in rabbit liver is mediated by MKK7. *FEBS Lett* 1997; **418**(1-2): 144-8.
41. Haeusgen W, Herdegen T, Waetzig V. The bottleneck of JNK signaling: molecular and functional characteristics of MKK4 and MKK7. *Eur J Cell Biol* 2011; **90**(6-7): 536-44.
42. Biankin AV, Waddell N, Kassahn KS, et al. Pancreatic cancer genomes reveal aberrations in axon guidance pathway genes. *Nature* 2012; **491**(7424): 399-405.
43. Koboldt DC, Fulton RS, McLellan MD, et al. Comprehensive molecular portraits of human breast tumours. *Nature* 2012; **490**(7418): 61-70.
44. Curtis C, Shah SP, Chin S-F, et al. The genomic and transcriptomic architecture of 2,000 breast tumours reveals novel subgroups. *Nature* 2012; **486**(7403): 346-52.
45. Bjorkblom B, Ostman N, Hongisto V, et al. Constitutively active cytoplasmic c-Jun N-terminal kinase 1 is a dominant regulator of dendritic architecture: role of microtubule-associated protein 2 as an effector. *J Neurosci* 2005; **25**(27): 6350-61.
46. Chang L, Jones Y, Ellisman MH, Goldstein LS, Karin M. JNK1 is required for maintenance of neuronal microtubules and controls phosphorylation of microtubule-associated proteins. *Dev Cell* 2003; **4**(4): 521-33.

47. Fey D, Halasz M, Dreidax D, et al. Signaling pathway models as biomarkers: Patient-specific simulations of JNK activity predict the survival of neuroblastoma patients. *Sci Signal* 2015; **8**(408): ra130.
48. Wada T, Joza N, Cheng HY, et al. MKK7 couples stress signalling to G2/M cell-cycle progression and cellular senescence. *Nat Cell Biol* 2004; **6**(3): 215-26.

7. Appendix

7.1. List of Figures

7.2. List of Tables